Annex 2 to final report
under ISTC Project No.3690

POST-TEST ANALYSIS OF MATERIAL STUDIES OF VVER-1000 MODEL ASSEMBLY TESTED AT THE PARAMETER-SF3 EXPERIMENT UNDER THE CONDITIONS OF SEVERE ACCIDENT WITH TOP FLOODING

2009

Abstract

The studies were performed according to the Work Plan for ISTC Project No.3690 “Study of fuel assemblies under severe accident top quenching conditions in the PARAMETER-SF test series”.

The report presents the results of material studies of a 19-rod model assembly of VVER-1000 after the PARAMETER-SF3 experiment under the conditions of initial stage of severe accident with the top quenching of FA overheated to 1600°C.

The objective of material studies was a description of the post-test state of the model assembly and analysis of its components (structure, degree of oxidation, fragmentation).

The studies included the following:

- description of external appearance, encapsulation and sectioning of the model FA;
- preparation of cross section slabs;
- optical and electronic microscopy;
- analysis of the obtained results.

The report includes 55 pages, 2 Tables, 43 Figures.

CONTENTS

INTRODUCTION

SF3 experiment was performed with the aim of studying the behaviour of a 19-rod model FA of VVER-1000 under simulated severe accident conditions. In the experiment the initial stage of severe accident was simulated with large coolant leak from the primary circuit of VVER-1000 RP when the core drying occurs as well as its heating-up to ~ 1600°C and top water quenching.

The main purposes of the experiment were:

- Study of behaviour of structural components of a 19-rod model FA of VVER-1000 (fuel pellets and claddings, shroud, periphery rods, spacer grids);
- Study of temperature evolution of cooling a 19-rod model FA of VVER-1000 overheated to ~ 1600°C with top quenching;
- Study of oxidation degree of structural components of a 19-rod model FA of VVER-1000;
- Study of interaction and structural-phase changes in the materials of a model FA of VVER-1000 (fuel pellets and claddings);
- Study of hydrogen release.

General purposes of the experiment governed the aims and tasks of material studies and namely:

- description of state of the model FA structural components;
- determination of thickness of oxide layers of fuel rod claddings and their distribution over FA height;
- quantitative evaluation of hydrogen mass generated during the experiment on the basis of the results of material studies.

Material studies were performed according to the Work Plan for ISTC Project No.3690 “Study of fuel assemblies under severe accident top quenching conditions in the PARAMETER-SF test series”.

1. DESCRIPTION OF POST-TEST STATE OF THE ASSEMBLY

In the course of dismounting of the test section and preparing the FA for encapsulation the assembly lower part (from 1300 mm and below) separated from the upper part and the personnel was forced to withdraw it out of the shroud. The assembly appearance is presented in Figs. 1, 2 (fuel rod 3.5 from the top), Table 1, and the detailed description is given below.

Up to the elevation of Z~500 mm the fuel rod claddings are covered with bright black layer of oxide. No assembly damages and differences in oxidation of fuel rods are observed.

With increase in elevation the oxide layer changes smoothly from bright black colour to white colour and oxide spallation is observed as well. The hottest zone of the assembly (Z~900…1300 mm) is considerably oxidized, fuel rod claddings have multiple damages (in the form of cracks and cleavages – fragments fell out).

At the elevation of Z~1300 mm, only several fuel rods are available for material investigations mainly due to the assembly withdrawal.

The assembly and the shroud cross-section slabs reveal no melting.

The state of spacer grids is the following:

- grid No.1 (Z = 1285-1305 mm) is completely damaged and no its fragments are found at this elevation;

- grid No.2 (Z = 1010-1030 mm), only 2 fragments are available. The main fragment around fuel rods 3.3 and 3.4, keeping the initial width (20 mm) (Figs.1f, 2a), is located 215 mm above grid No.3 (Z = 735-755 mm). A small fragment with width of 5…8 mm at fuel rod 3.2 is located 170 mm above grid No.3. No ring for spacing the given grid and the shroud is found;

- grid No.3 is fragmented into two parts (Fig.1d, e). A fragment around fuel rods 3.2 – 3.6 corresponds to the design location. At fuel rods 3.8, 3.11 3.12 and 3.1 grid No.3 cells are missed. In the region of fuel rods 3.7, 3.9 and 3.10 there is the second fragment of the grid displaced by 12 mm downwards. The ring for spacing the given grid and the shroud remains in the form of a sector from fuel rod 3.1 to fuel rod 3.8 and is displaced (Fig.1d);

- a pitch between grids Nos. 4, 5 and 6, located below, corresponds to the design value of 255 mm. Rings for spacing the grids and the shroud are located at place.

The state of periphery rods over the assembly (two rods on each side) corresponds to the state of claddings of fuel rods of the third row with respect to the

tendency of change in colour and spallation of oxide scale. However the following peculiarities are revealed:

- some periphery rods are intact practically over the whole FA and there is a break at the elevation of Z ~ 1200…1350 mm (5 pcs.);

- other seven periphery rods are damaged at the considerably lower elevations (approximately in the region of grid No.3, Fig.1d). Evidently, this is caused by the fact that periphery rods were fastened to grids rather tightly and due to complete damage of grids Nos 1 and 2 during withdrawal of the assembly their break occurred under bending.

The assembly upper part Z~1300…1500 mm is also considerably oxidized, the fuel rod claddings are covered with porous (flaking and easily spalling) zirconium oxide to the elevation of Z ~ 1550 mm. Many fuel rods are fragmented, there are no input leads inside them (fell out due to break-off of the assembly during disassembling procedure). Identification of numbers of claddings of this assembly part turned to be impossible due to considerable displacements of fuel rods.

Visual examination of the model FA shroud after its withdrawal from the test section showed that its outside surface is covered with compact black thin zirconium oxide layer. From the elevation of ~ 900 mm and up to 1300 mm the through-wall cracks were revealed and the shroud exhibited a tendency to break off. The shroud integrity was kept with quick-solidifying compound laid on the outside. Later the shroud was filled with epoxy resin.

2. METHODS OF MATERIAL STUDIES

2.1. Methods of encapsulation and sectioning of the model FA

After visual inspection and photo documentation of the assembly appearance it was placed into a plastic vessel and filled with a compound (epoxy resin ЭД-20) in horizontal position. For spacing the fuel rods of the third row of the assembly and the vessel walls the copper bands were used, Fig. 3, 4 (Z = 800 mm).

After solidifying the compound the assembly was withdrawn from the plastic vessel and cut into slabs. The cuts were done with cutting-off machine Delta-Abrasimet with diamond blade of thickness 1.7 mm. Thickness of cross section slabs was chosen to be 15…20 mm to be ensured in their integrity keeping during their cutting out (to avoid their transverse cracking and spilling out of FA components). The exact values of cross-section slabs coordinates are presented in Table 2. The places of cutting out the blades were determined according to the methods of material studies described below.

To remove voids and cavities remained after FA filling with the compound the cross section slabs vacuum impregnation was made with epoxy resin EPO – THIN at the “Buehler” impregnator. Then the cross section slabs have been ground and polished.

The macro photos of the ground cross-section slabs were taken by the digital camera SONY (8 mps) (Fig. 3, 4). Further on, the available macrographs were used for comparative evaluation of the degree of the assembly damage at different elevations.

2.2. Methods of material studies of the model FA

During development of methodical approaches for material studies of the assembly the greatest attention was directed to the cross-sections wherein temperature measurements were conducted in the course of the experiment.

Analysis of the experiment results showed that the highest temperatures in the assembly were reached on claddings of fuel rods of the 2^{nd} row at the elevation of Z ~ 1300 mm. Fig. 5 presents cladding temperature distribution over heated zone for 2^{nd} and 3^{rd} rows rods, restored by the method of interpolation by indications of thermocouples, at the beginning of pre-oxidation stage (t = 9760 s), at the beginning of the transient stage (t = 13725 s), at the moment of electrical power switching off (t = 14486 s) and before flooding onset (t = 14481 s). Temperature points at the elevations correspond to thermocouples indications at the corresponding time moments. In the lower part of the assembly (0 – 400 mm) the relatively low temperatures (with regard to oxidation process) were recorded. Maximum temperature in the assembly

lower part (0 – 400 mm) in the course of the experiment did not exceed ~ 850°C (Fig. 5a, b) that suggests low oxidation degrees. Results of studies of the oxidation degree of fuel rods claddings and shroud in this area confirmed the given conclusions. Thickness of oxide layer on claddings and shroud at the elevation of Z = 400 mm is not high and corresponds to ~ 2…10 μm.

The main attention in post-test studies was directed to the FA middle (500 – 800 mm) and upper (900 – 1500 mm) parts. For metallographic studies, 12 cross section slabs were chosen and prepared from these elevations.

In the middle part (500 – 800 mm) of the assembly the maximum temperatures of the 2nd row claddings did not exceed 1300°C (Fig. 5). According to indication of the thermocouples the pre-oxidation phase claddings of the 2nd row were held at temperatures of 800-950°C. For metallographic measurements of cladding thicknesses of oxide and metal layers four cross section slabs were selected from elevations of 500, 600, 700 and 800 mm (Table 2, Fig. 3). Description of the state of the assembly components in this zone was made for the cross-section slabs from the elevations of 500 and 800 mm.

According to the results of temperature measurements, the hottest zone location was observed in the assembly upper part at 1250-1300 mm elevations (Fig. 5) and so, the highest degree of oxidation of the shroud and claddings would corresponds to this zone. Metallographic measurements of layers thickness at the upper part of the bundle were done with more detail (in cross section slabs from the elevations of 900, 1000, 1100, 1200 1250 and 1300, 1400 and 1500 mm, Table 2, Fig. 3, 4). Description of the state of the assembly components in this zone was made for cross-section slabs from the elevations of 1000, 1200 and 1300 mm.

Just during visual examination of the assembly it became clear that direct measurement of the zirconium dioxide layer thickness on cladding surfaces are not available along the whole assembly length (500-1500 mm) due to pronounced spalling of oxide scale (only at the elevation of 400 mm the direct measurements of oxide thickness were performed because of the claddings reveal no spalling). In this case the only method for assessment of oxidation degree of claddings is evaluation by thickness of the remaining metal layer. Difference between the initial cladding thickness and the measured thickness of the remaining metal part, considering Pilling-Bedworth factor reflecting the change in volume during transformation of metal to oxide, gives the oxide thickness. This procedure is widely used, for instance, in QUENCH-12, PARAMETER-SF2 tests, however for the assembly in PARAMETER-SF3 test its modification was

required. The matter is that in the course of the experiment PARAMETER-SF3 within the time interval from ~5000 s to 14500 s the pressure was increasing inside fuel rods and so the pressure differential on claddings was 0.1…0.3 MPa (Fig. 5c). At the beginning of the experiment (when the claddings were not oxidized practically), this pressure differential led to their deformation in the form of ballooning, and consequently, to cladding thinning. As the cladding deformation is nonuniform over the length and azimuth of each fuel rod, the additional measurements of inner diameters were required for each cladding at all selected cross-sections.

On the whole, the procedure of calculation of oxide layer thickness on surface of the deformed claddings included the following:

1. Measurements of thickness of metal layers and inner diameter of claddings in all cross-section slabs studied (Table 2);

2. Calculation of thickness of the deformed claddings (basing on the assumption of absence of axial deformation);

3. Calculation of thickness of ZrO_2 layer as a difference between thickness of the deformed cladding and the measured residual metal layer considering Pilling-Bedworth factor.

In addition to the measurements of thickness of metal layers and inner diameter of claddings, the given work deals with measurements of thickness of dense oxide scales and α-Zr(O) layers on the outer and inner surfaces of fuel rod claddings.

Measurements in each slab were performed for each cladding. Layer thickness was measured in four directions, as a minimum, inner diameter - in two directions.

Studies of the shroud were also performed using cross-sections of Z = 0, 600, 700, 800, 900, 1000, 1100, 1200, 1250 and 1300 mm (9 pcs., in all). In each section in eight directions, as a minimum, the measurements were performed of the remaining metal part of the shroud and also of the thickness of dense oxide and α-Zr(O) layers on the shroud outer and inner surfaces. Measurements of the shroud geometrical dimensions (in cross-section at the height of 0 mm) showed that its inner diameter is 67 mm, and wall thickness varies from ~1.14 to ~1.19 mm. The procedure used for calculation of zirconium dioxide thickness as a difference between thickness of the shroud wall and the measured metal part, considering Pilling-Bedworth factor, is rather sensitive to change in the shroud thickness. It can be supposed that various thickness of the shroud is also available in other cross-sections; however the original thickness in each cross-section is unknown. Besides, in the course of the experiment the shroud was damaged [1], with this, its deformation could occur and influence its

geometrical characteristics. However, these characteristics were impossible to be determined. Therefore, as the initial data for calculation of zirconium dioxide thickness the wall thickness and inner diameter of the shroud were assumed equal to the corresponding values measured in cross-section at the elevation of 0 mm, possible shroud deformation was neglected. The mentioned assumptions and simplifications undoubtedly lead to an error in the calculated thickness of zirconium dioxide; however its value is governed mainly by the shroud wall thickness deviation.

On the basis of the measured data cladding deformations over heated zone, residual metallic layer thickness and dense oxide thickness axial profiles for claddings and shroud were plotted.

Metallographic analysis of cross-section slabs was performed with the optical microscope OLYMPUS using the computer code package OMNIMET. Electron microscope studies of cross-sections were performed with the scanning electron microscope JEOL JSM – 6460 LV.

3. RESULTS OF MATERIAL STUDIES

3.1. Structural analysis of cross-sections

3.1.1. Elevations of 500 – 800 mm

At Z = 500 mm elevation (top view) there are practically no visible damages of the assembly (all fuel rod claddings, periphery rods and 4 thermocouples were kept in original arrangement, the claddings maintained the integrity, Fig. 6, 7). Maximum temperature of claddings at this elevation at the pre-oxidation stage did not exceed ~ 750°C, and before flooding onset ~ 950°C (Fig. 5). There are cracks on some pellets of uranium dioxide. In some pellets there are no fuel fragments (Fig. 7). However, crumbling of pellets occurred probably in the course of the assembly sectioning or preparing the cross-section slabs for metallographic examinations. In fuel rods 2.4, 3.7 and 3.8 there are no heaters and fuel pellets which fell out during FA handling.

On most fuel rods the oxide scale is thin and well connected with metal (the fuel rods have black and bright appearance), and only some of them (fuel rods 2.5, 2.6, 3.10, 3.11 and 3.12) reveal multilayered spalled off scale (as to the external appearance of fuel rods, they are dark mat or grey) (Fig. 8). Thinning of the cladding metal part reached ~ 670…620 μm.

Structural state of the claddings at the given elevation is characterized by the following:

- calculated thickness of oxide scale on the cladding external surfaces is 10 - 60 μm (stronger oxidation was observed only on some fuel rods 2.5, 2.6, 3.10, 3.11, and 3.12 with spalled off scale);

- the measured thickness of zirconium oxide, tightly bound with cladding, varies within the range of 4 – 9 μm.

The remained metal part of claddings consists of two layers: α - Zr(O) with thickness of not more than 30 μm and β - Zr.

Calculated thickness of oxide scale on periphery rod surfaces is ~ 15 μm (in most cases ~ 5 μm and in one case ~ 40 μm).

Results of measurements of thickness of the remained metal part of claddings at Z = 500 mm elevation are shown in Fig. 10. Calculated values of oxide layers are given in Figs. 37, 38.

At Z = 800 mm elevation (top view) the bundle elements arrangement is distorted significantly (the displacement of fuel rods 3.12 and 2.6 as compared to their original location is observed, fuel rod 3.10 is absent due to break off, there are no heaters and fuel in fuel rods 2.4, 3.7 and 3.8 due to break off, there are five periphery rods, Fig. 11).

In the given section a fragment of spacer grid (on fuel rod 3.7), a fragment of fuel rod cladding (near fuel rod 3.11) were revealed, as well as many oxide scales remnants which fell down apparently from FA upper elevations. Fragmentation of some fuel rod claddings was observed – claddings of fuel rods 2.6 and 3.12 were damaged (i.e. practically absent in the given section), there are no fragments of claddings of fuel rods 3.1 and 3.11.

Maximum cladding temperatures at this elevation at the pre-oxidation stage did not exceed ~ 1050°C, and before flooding onset ~ 1300°C (Fig. 5).

The third row fuel rod claddings exhibit pronounced local non homogeneous cladding oxidation: rods 3.3, 3.4, 3.5, and 3.6 are oxidized weaker than others (Fig.16a). Heaters in these rods failed during the experiment that suggests effect of heater failure on claddings oxidation. However, significant oxidation inhomogeneity for rods with unfailed heaters cannot be explained with this assumption (for example, residual metallic layer thicknesses measured on rods 2.1 and 2.5 differ by factor two). Besides, similar oxidation inhomogeneity was found in SF2 test in which heater failures did not occur (Fig. 18 [3]).

On all fuel rods the considerable oxide spallation is observed (Fig.13).

No fuel-clad interaction is revealed. Oxidation of inner surface of fuel rod claddings is insignificant.

Periphery rods (Fig.14) and inner surface of the shroud in the given section are oxidized non-homogeneously as well: calculated thickness of oxide scale on the surface of periphery rods varies within the interval of 20 – 470 μm, and on the shroud 50 – 240 μm.

In the given section a fragment of spacer grid is revealed also (near fuel rod 3.7) with spalled off oxide on its surface and through cracks in metal part (Fig. 15).

Thickness of cladding metal layer varies from 635 to 330 μm.

Structural state of claddings at the given elevation is characterized by the following:

- calculated thickness of oxide scale on the cladding outer surfaces is 60… 500 μm;

- the measured thickness of zirconium oxide, tightly bound with cladding and having columnar structure, varies within the range of 12…250 μm.

The remained metal part of claddings consists of two layers: α - Zr(O) with thickness of 10…150 μm and β - Zr.

The generalized results of measurements of thickness of the remained metal part of claddings for different fuel rods at Z = 800 mm elevation are shown in Fig. 16. Calculated values of oxide scale - in Figs. 37, 38, 42.

3.1.2. Elevation interval of 900 – 1300 mm

At Z = 1000 mm elevation (top view) considerable assembly damage was observed. 12 fuel rods 2.1, 2.2, 2.3, 2.5, 2.6, 3.1, 3.2, 3.3, 3.4, 3.5, 3.6, 3.11 and five periphery rods are available for examinations after handling (Fig. 17). In the given section a fragment of spacer grid was revealed (obviously SGr No.2, Z = 1010 – 1030 mm, near fuel rods 3.3 and 3.4), as well as zirconium sheath of thermocouple (between fuel rods 3.1, 3.2 and 2.2). Maximum cladding temperatures at this elevation at the pre-oxidation stage did not exceed ~ 1100°C, and before flooding ~ 1350°C (Fig. 5). Structural components oxidation inhomogeneity also takes place at the given level (Fig. 20).

Typical oxidation state of fuel rod claddings is shown in Fig. 18. On their surface there is an easily spalled off layer of ZrO_2, under which one can see dense oxide with columnar structure well connected with metallic substrate (Fig. 19). In α - Zr(O) layer there are numerous radial not oxidized cracks penetrating into β - phase (Fig. 19). Some fuel rods have through-wall cracks; fuel relocation and fuel-clad interaction are not revealed. There is internal oxidation in some fuel rod claddings but it is insignificant.

Calculated thickness of oxide scale on surface of periphery rods varies within the interval of 140 – 540 μm, and on shroud internal surface to be 50 – 320 μm.

Thickness of cladding metal part varies from 580 to 300 μm.

Structural state of claddings at the given elevation is characterized by the following:

- calculated thickness of oxide scale on the cladding outer surfaces is 290…510 μm;

- the measured thickness of columnar zirconium oxide, well connected with metallic layer , varies within the range of 30…180 μm.

The remained metal part of claddings consists of two layers: α - Zr(O), with thickness of 20…350 μm, and β - Zr.

The generalized results of measurements of thickness of the remained metal part of claddings for different fuel rods at Z = 1000 mm elevation are shown in Fig. 21. Calculated values of oxide scale are given in Figs. 37, 38, 42.

At Z = 1200 mm elevation (top view) further increase in the oxidation degree of fuel rod simulators and their damages are observed (Fig. 22). At this cross-section six fuel rods (fuel rods 2.2, 3.2, 3.3, 3.4, 3.6, 3.11), and five periphery rods are available for measurement. The other fuel rods and periphery rods were lost due to manipulations with the bundle mentioned above. Claddings maximum temperature at this elevation at the pre-oxidation stage did not exceed ~ 1300°C, and before flooding onset – ~ 1500°C (Fig. 5). Typical oxidation state of fuel rod simulators is shown in Fig. 23. On their surfaces there is also easily spalled off ZrO_2 oxide, under which there is dense oxide well connected with metal layer (Fig. 21). Owing to brittleness of sub-oxide layer, all fuel rods practically have a large number of cracks non-oxidized (Fig. 23), in claddings the through-wall cracks are observed (Fig. 24), and some claddings (fuel rods 3.2, 3.3) are fragmented. However no fuel-clad interaction is revealed also.

There is internal oxidation in some fuel rod claddings, with this, the measured thickness of oxide layer reaches ~ 2…5 μm.

Calculated thickness of oxide scale on the surface of periphery rods varies within the interval of 380 – 650 μm, and on the shroud internal surface to be 70 – 300 μm.

Thickness of cladding metal part varies from 520 to 325 μm.

Structural state of claddings at the given elevation is characterized by the following:

- calculated thickness of oxide scale on the cladding outer surfaces is 250…490 μm;

- the measured thickness of columnar zirconium oxide, tightly bound with cladding, varies within the range of 50…300 μm.

The remained metal part of claddings 3.2, 3.3, 3.4 and 3.6 consists of two layers: α - Zr(O) with thickness of 50…350 μm, and β - Zr, in claddings 2.2 and 3.11 the α - Zr(O) sublayer occupies whole metal part.

The generalized results of measurements of thickness of the remained metal part of claddings for different fuel rods at Z = 1200 mm elevation are shown in Fig. 26. Calculated values of oxide scale are given in Figs. 37, 38, 42.

At Z = 1300 mm elevation (top view) the maximum damages are observed because this is hottest zone (Fig. 27). In the cross-section three periphery rods and six fragments of claddings of fuel rods are available for measurements. Due to severe damages of FA and very strong arrangement distortion, available claddings cannot be identified. Maximum temperature of claddings at the pre-oxidation stage did not exceed

~ 1300°C, and before flooding onset ~ 1600°C (Fig. 5). Typical oxidation state of fuel rod simulators is shown in Fig. 28.

Oxidation character of fuel rod claddings is the following (Fig. 29):

- on outer surface of claddings there is multilayered easily spalled off zirconium oxide of white colour;

- under this layer there is a dense oxide with columnar structure (dark grey). There are cracks and splitting in it (Fig. 29), its thickness varies within 200 – 500 μm;

- on three claddings in this section (their number in the scheme are 6, 7 and 8) two different layers are visually recognized in dense columnar oxide. In the internal layer (on metal substrate) precipitations of the second α - Zr(O) phase are revealed along columnar grain boundaries of ZrO_2 layer, that is evidently indicative of high-temperature (above 1500 °C) oxidation and formation of ZrO_2 cubic phase, [2]. Thickness of this sub-layer is 100 – 300 μm;

- the whole metal part of claddings at this cross-section presents the α - Zr(O) sub-layer with through cracks;

- internal oxidation of claddings at this elevation is insignificant, oxide thickness varies within 0 – 15 μm, melting and fuel-clad interactions are not revealed. Average oxide thickness (calculated by residual metallic layer thickness) is ~340 μm. The generalized results of measurements of thickness of the remained metal part of claddings for different fuel rods at Z = 1300 mm elevation are shown in Fig. 31.

Zirconium periphery rods are covered with multilayered oxide (Fig. 30). On the outer surface the oxide is easily separated. The oxide central part is multilayered with splitting and radial cracks. Oxide well connected with metal substrate is of dense columnar structure. Oxidation of periphery rods over the perimeter is irregular, i.e. with pronounced local area strong oxidized.

Calculated thickness of oxide scale on surface of periphery rods varies within the interval of 450 – 740 μm, and on the shroud internal surface to be 120 – 330 μm.

The generalized results of measurements of thickness of the remained metal part of claddings for different fuel rods at Z = 1300 mm elevation are shown in Fig. 31. Calculated values of oxide layers are presented in Figs. 37, 38, 42.

3.2. Distribution of fuel rod cladding deformation over heated zone

By the results of measurements of inner diameters of fuel rod claddings at all studied cross-sections the calculation of outer diameters of deformed claddings was performed (based on the assumption of absence of axial deformation), and the circumferential deformation was calculated for each cladding in each section analyzed (as a ratio of cladding diameter increase to the origin diameter of non-deformed cladding).

By the results of the performed calculations and averaging the values (for fuel rods of the second and third rows, respectively) distribution of circumferential deformation over heated zone are plotted (Fig. 32). Maximum circumferential deformation of claddings of fuel rods of the second row is located at the elevation of ~ 800 mm and equal to ~ 9.5%, and for fuel rods of the third row – at the elevation of ~ 1000 mm and equal to ~ 10%, that should be considered in calculation of volume of the zirconium oxide formed (because the deformation leads both to thinning of cladding and to increase in its diameter).

3.3. Distribution of oxidation of fuel rod claddings and shroud over the assembly height

Measurements of thickness of the dense oxide and the remaining metal part of claddings were made on each fuel rod and, as a minimum, in four azimuth directions if possible (because in some cases fragmentation of claddings occurred). At the elevations of 1300, 1400 and 1500 mm it was difficult to identify fuel rods due to FA damages, and owing to this fact the data for these elevations are given in plots for renumbered claddings.

Results of measurements and of calculation of oxide scale thickness are presented in Figs. 33-38 separately for the second and third row claddings for convenient analysis.

Analysis of the results of measurements showed pronounced non homogeneous cladding oxidation across the bundle.

For the analysis of tendency to growth of zirconium dioxide thickness on surfaces of fuel rod claddings the distribution of averaged calculated thickness of oxide scale on cladding surfaces over heated zone is plotted (Fig. 39). Maximum thickness of zirconium dioxide is 530 μm at the elevatin of 1300 mm.

It should be noted that due to considerable deformation of claddings the oxide scale thickness, measured in SF3 experiment, should be used for verification of

computer codes if both only both cladding deformation and oxidation models are initiated (consideration of geometrical factor).

Fig. 43 presents the distribution of zirconium dioxide volume.

It follows from the analysis of Figures 39 and 43 that in spite of considerable deformation of claddings the axial profiles of averaged thickness of oxide scales and of oxide volume are similar and both profiles confirm the results of temperature measurements concerning location of the hottest area at the elevation of 1300 mm.

It is significant that in both profiles the local minimum can be seen at the elevation of 1200 mm, though it contradicts the temperature profile.

In studying the shroud the measurements of thickness of metal part and dense oxide were performed in eight directions. The results of measurements (following their averaging in each section) and of the calculation of oxide thickness are presented in Figs. 40 – 42. As seen from the Figures, the location of the thickest oxide (1300 mm) corresponds to the location of the hottest area in FA.

3.4. Evaluation of hydrogen mass

On the basis of obtained results of the bundle metallographic studies upper limit of hydrogen mass, that could be generated in the course of SF3 experiment, was estimated.

Oxidation of the following assembly components was taken into account (in the order of their contribution into the total hydrogen mass released):

1) fuel rod claddings at Z = 400…1500 mm elevations and periphery rods at Z = 400…1300 mm elevations;
2) shroud at Z = 600…1300 mm elevations;
3) zirconium sheath of thermocouples;
4) spacer grids (Nos.1 and 2);
5) tantalum heaters.

Oxidation of fuel UO_2, thermocouple wires, structural components of the test section upper part were neglected in the evaluations.

It should be considered that after handling part of structural components was lost. Especially it concerns the hottest elevations (1250 - 1300 mm) where not more than 30% of claddings are available. Of course, the authors of the report understand that we have few data to evaluate if the available claddings and peripheral rods are representative. Nevertheless, with no alternative available, the evaluation of oxidation extent of components (claddings, periphery rods) at these elevations was made basing

on assumption that the average oxidation degree of the lost components is comparable to the average oxidation degree of the available components.

The amount of hydrogen that could be generated due to oxidation of fuel rod claddings was evaluated by the oxygen mass in the α - Zr(O) and ZrO_2 layers. With this, the changes in geometry of claddings (increase in diameter and wall thinning caused by deformation) were considered and it was also assumed that the formed zirconium dioxide layer is stoichiometric, oxygen content in α - Zr(O) was assumed to be 30% atm. Thickness of α - Zr (O) layer was evaluated with the accuracy of 10…20 μm. Oxygen content in claddings below 400 mm was neglected due to small thickness of oxide layers. Figure 43 provides the result of evaluation of the assembly different sections contribution into hydrogen release that was obtained by direct recalculation of the evaluated oxide volumes. Considering the given assumptions, the hydrogen mass from oxidation of claddings and periphery rods was estimated to be ~ 28.3 g (22 g from claddings, 6.3 from periphery rods).

Uncertainty of hydrogen mass evaluation due to shroud oxidation is connected with azimuthal non-uniformity of its thickness. Evaluation of hydrogen mass by the residual metal layer thickness assuming average wall thickness to be 1.17 mm gives the value of 7.6 g. This value would be considered to be acceptable considering that estimated mass deviation due to shroud thickness deviations to be 1.14-1.19 mm are not high (corresponding hydrogen mass are equal 6.8 g and 8.5 g). Hydrogen mass estimated by thickness (volumes) of dense zirconium dioxide and alpha-zirconium layers directly measured on the shroud is equal to 2.48 g.

Thermocouples are not available in the cross-sections. So oxidation of zirconium sheath of thermocouples was evaluated considering their arrangement assuming that average oxidation degrees of sheath materials and claddings at the same elevations are similar. By the results of such evaluation hydrogen mass due to oxidation of thermocouple sheath does not exceed 1.9 g.

During the experiment, the SGrs No.1 and No.2 were oxidized practically completely. Due to oxidation of the grids ~ 2 g of hydrogen could be generated assuming the whole amount of zirconium is transformed into stoichiometric oxide.

The studies of structure of heaters showed that hydrogen generation due to their oxidation does not exceed 1.5 g.

So, the total hydrogen amount, that could be generated due to assembly materials oxidation in the course of the experiment, does not exceed ~ 42 g. Evaluation of hydrogen absorption owing to hydrogen absorption by claddings and shroud metal

layers was not made because special sample treatment are needed for X-ray used for this purpose but it cannot be done due to strong SF3 bundle material embrittlement.

CONCLUSIONS

Analysis of post-test material studies showed that:

- the state of the lower part of heated zone (Z = 0…400 mm) does not practically differ from the original state, and oxide thickness on the claddings external surface does not exceed 2-10 μm;

- within the range of 500…1300 mm elevations the bundle reveals breakaway oxidation;

- in the middle part of heated zone (Z = 500…800 mm) the fuel rod simulators are displaced relative to the original position in the assembly cross-section, the external cladding surfaces are covered with multilayered zirconium oxide, separating from metal surface, and its thickness on some fuel rods (at 800 mm elevation) reaches ~ 400 μm.

In the upper part of heated zone (Z = 900…1300 mm) the rods arrangement is greatly distorted. The claddings are oxidized both on the external (to 550 μm), and on the internal (to 50 μm) surfaces. Zirconium dioxide has different morphology. The internal part of the oxide scale is dense zirconium oxide of columnar structure well connected with the metal surface, that was grew, evidently at the transient phase. Its thickness increases with increase in elevation and reaches the maximum value at 1250 – 1300 mm elevation. Distribution of its thickness through the assembly section at the given elevations is considerably nonuniform and varies within the range of 100…350 μm. In the hottest zone precipitations of the second α - Zr(O) phase are revealed in dense oxide of three fuel rods that, evidently, is indicative of their high-temperature (above ~1500°C) oxidation and formation of cubic ZrO_2 phase. The dense dioxide is covered with the external zirconium dioxide of multilayered structure detached from the cladding. Metal part of claddings is α phase stabilized with oxygen (α - Zr (O)). Fuel rod claddings are embrittled, i.e. have the through-wall cracks, and fragmented. No fuel-clad interactions are revealed in the assembly.

In the studied assembly cross-sections considerable non-homogeneous oxidation of claddings is observed.

Thickness of zirconium dioxide on surfaces of fuel rods and shroud, calculated on the basis of measurements of metal layer thickness, confirm indications of thermocouples on location of the hottest area at the elevation of 1300 mm.

Upper amount of hydrogen mass that could be released due to oxidation can be estimated to be ~42 g. To compare the calculated hydrogen mass with the measured

one it is necessary to consider additionally mass of hydrogen absorbed by FA components, at least, due to the shroud hydrogenation.

REFERENCES

1. Protocol of PARAMETER-SF3 Experiment Results.
2. Results of the QUENCH – 12 experiment on reflood of a VVER – type bundle. J.Stuckert, A. Goryachev, etc.
3. Analysis of Material Studied of WWER-1000 Model Assembly Tested at the PARAMETER-SF2 Experiment under the Conditions of Severe Accident with Top and Bottom Flooding.

APPENDIX

Table 1

Description of fuel rods appearance of the model assembly PARAMETER-SF3 on visual inspection

Fuel rod No.	Description of fuel rod state
1.1	Visible inspection is impossible, prevented by periphery rods and third row of fuel rods.
2.1	Visible inspection is impossible, prevented by periphery rods and third row of fuel rods.
2.2	Beginning from Z ~ 600 mm elevation the cladding colour changes smoothly and oxide flaking occurs, from Z ~ 630 mm the cladding becomes white with strong flaking. At Z ~ 845 mm elevation – a crack, at Z ~ 930 and 1160 – large chips, from Z ~ 1220 mm elevation and above the cladding is failed.
2.3	Beginning from Z ~ 710 mm elevation the cladding colour changes and oxide flaking occurs. At Z ~ 800 mm the cladding becomes white, from Z ~ 1130 mm elevation and above the cladding is failed.
2.4	At Z~550 mm elevation the oxide flaking is started with changing of cladding colour, from Z~ 890 mm elevation and above the cladding is failed.
2.5	From Z ~ 1150 mm elevation and above the cladding is failed. On fuel column the cladding fragments are observed.
2.6	The fuel rod is not available for visible inspection up to the elevation of Z ~ 670 mm, and above there is a white cladding with oxide flaking. Within the range of Z ~ 700…720 mm the cladding chip is observed, from Z~ 800 mm elevation and above the cladding is failed.
3.1	From Z ~ 570 mm elevation the fuel rod cladding changes its colour smoothly from black to white with traces of oxide flaking. Within the range of Z ~ 850…920 mm there is no external sector of fuel rod cladding. At Z ~ 1045 and 1155 mm elevations the cladding has radial cracks. From Z ~ 1185 mm elevation the cladding is failed.
3.2	Beginning from Z ~ 640 mm elevation and above the oxide flaking is observed, and from Z ~ 745 mm the cladding changes its colour completely. At Z ~ 865 mm – radial crack, Z ~ 990…1070 mm – longitudinal crack, from 1230 mm elevation and above - the cladding is failed
3.3	At Z ~ 740 mm elevation the oxide flaking is observed, and at Z ~ 810 mm the cladding colour changes. At Z~930…1050 mm elevations spallation and separation of the cladding layers are observed (under porous white oxide the dense dark grey oxide is observed), and from Z ~ 1200 mm elevation and above the cladding is failed.
3.4	From Z ~ 800 mm elevation the cladding colour changes smoothly from grey to white with occurrences of the oxide flaking. At Z ~ 1140…1170 mm separation of the oxide from the cladding is noticeable, above Z ~ 1245 mm. At Z ~ 1263 mm the heater is broken.
3.5	From Z ~ 820 mm the smooth change in colour is started, and at Z ~ 900 mm the cladding becomes white with trances of the oxide flaking. At Z ~ 1100 mm the cladding is failed, the fuel column is observed, some pellets are fragmented and their parts are absent.

3.6	At Z ~ 800 mm the flaking appears, and from Z ~ 865 mm elevation the cladding becomes white. At Z ~ 1070 and 1175 mm there is a crack, at Z ~ 1125…1150 mm a chip of the cladding sector is observed. From Z ~ 1275 mm elevation the cladding is failed.
3.7	Beginning from Z ~ 665 mm the smooth change in the cladding colour is observed, and from Z ~800 mm the cladding becomes white with noticeable flaking. Failure is observed at Z ~ 965 mm elevation, and at Z ~ 1025 mm the heater is broken.
3.8	From Z ~ 680 mm elevation the cladding colour changes smoothly, and at Z ~ 930 mm the fuel rod is failed, the heater is broken.
3.9	At Z ~ 625 mm elevation the smooth change in colour is started and at Z ~ 670 mm the cladding is white. Within the range of Z ~ 750…775 mm the oxide is separated, at Z ~ 820,875 and 910 mm – cracks, from Z ~ 950 mm and above the cladding is failed, only the fuel column on the heater remains.
3.10	From Z ~ 500 mm elevation the oxide flaking is started with smooth change in the cladding colour, and at Z ~ 570 mm the cladding becomes white. At Z ~ 670 mm – break of the heater.
3.11	Beginning from Z ~ 550 mm the colour changes smoothly and oxide flaking appears on the cladding, within the range of Z ~ 660…760 mm no cladding is observed on fuel column and in the above part of fuel column the cladding fragments are observed.
3.12	From Z ~ 500 mm elevation the smooth change in colour and flaking are started, and from Z ~ 580 mm the cladding becomes white. At Z ~ 670 mm radial crack is observed, within the range of Z ~ 670…800 mm – longitudinal crack, further on - there are no cladding and heater.

Table 2

Coordinates of transverse cuts of the model FA in SF3

Specimen	Specimen length, mm	Specimen coordinate		Remarks
		Bottom, mm	Top, mm	
	0	0	0	
Cut	1.7	0	1.7	
	20.5	1.7	22.2	cross-section slab
Cut	1.7	22.2	23.9	
	68.3	23.9	92.2	
Cut	1.7	92.2	93.9	
	67	93.9	160.9	
Cut	1.7	160.9	162.6	
	51.7	162.6	214.3	
Cut	1.7	214.3	216	
	73.7	216	289.7	
Cut	1.7	289.7	291.4	
	16.2	291.4	307.6	

Cut	1.7	307.6	309.3	
	16.7	309.3	326	
Cut	1.7	326	327.7	
	54.2	327.7	381.9	
Cut	1.7	381.9	383.6	
	16.7	383.6	400.3	cross-section slab
Cut	1.7	400.3	402	
	75.7	402	477.7	
Cut	1.7	477.7	479.4	
	20.5	479.4	499.9	cross-section slab
Cut	1.7	499.9	501.6	
	78.1	501.6	579.7	
Cut	1.7	579.7	581.4	
	21.6	581.4	603	cross-section slab
Cut	1.7	603	604.7	
	76	604.7	680.7	
Cut	1.7	680.7	682.4	
	21.3	682.4	703.7	cross-section slab
Cut	1.7	703.7	705.4	
	74.9	705.4	780.3	
Cut	1.7	780.3	782	
	18.5	782	800.5	cross-section slab
Cut	1.7	800.5	802.2	
	58	802.2	860.2	
Cut	1.7	860.2	861.9	
	19.5	861.9	881.4	
Cut	1.7	881.4	883.1	
	21	883.1	904.1	cross-section slab
Cut	1.7	904.1	905.8	
	32.4	905.8	938.2	
Cut	1.7	938.2	939.9	
	38.4	939.9	978.3	
Cut	1.7	978.3	980	
	22	980	1002	cross-section slab
Cut	1.7	1002	1003.7	
	75.7	1003.7	1079.4	

Cut	1.7	1079.4	1081.1	
	18.5	1081.1	1099.6	cross-section slab
Cut	1.7	1099.6	1101.3	
	43.2	1101.3	1144.5	
Cut	1.7	1144.5	1146.2	
	34.3	1146.2	1180.5	
Cut	1.7	1180.5	1182.2	
	19.1	1182.2	1201.3	cross-section slab
Cut	1.7	1201.3	1203	
	26.7	1203	1229.7	
Cut	1.7	1229.7	1231.4	
	18.5	1231.4	1249.9	cross-section slab
Cut	1.7	1249.9	1251.6	
	21.2	1251.6	1272.8	
Cut	1.7	1272.8	1274.5	
	25.4	1274.5	1299.9	cross-section slab
Cut	1.7	1299.9	1301.6	
	47.1	1301.6	1348.7	

a (Z = 400…500 mm)

b (Z = 500…600 mm)

c (Z = 600…700 mm)

d (Z = 700…800 mm)

e (Z = 800…900 mm)

f (Z = 900…1000 mm)

Fig. 1. The SF3 bundle appearance (Z = 400-1000 mm) after withdrawal from the shroud (fuel rod 3.5 is located in the centre).

a (Z = 1000…1100 mm)

b (Z = 1100…1200 mm)

Fig. 2. The SF3 bundle appearance (Z = 1000-1200 mm) after withdrawal from the test section.

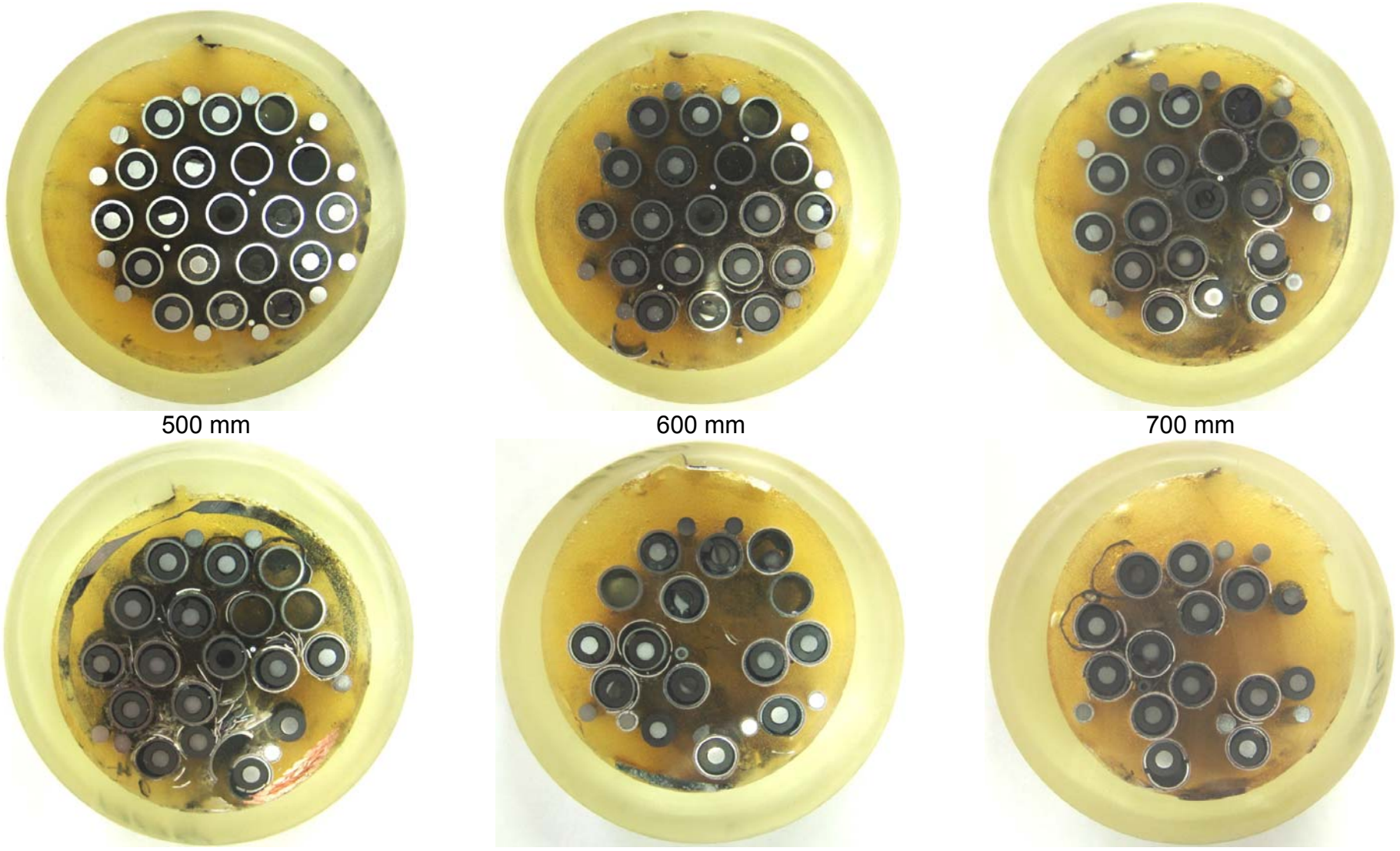

Fig. 3. Photos of the assembly cross-sections within the range of Z ~ 500…1000 mm elevations.

1100 mm

1200 mm

1250 mm

1300 mm

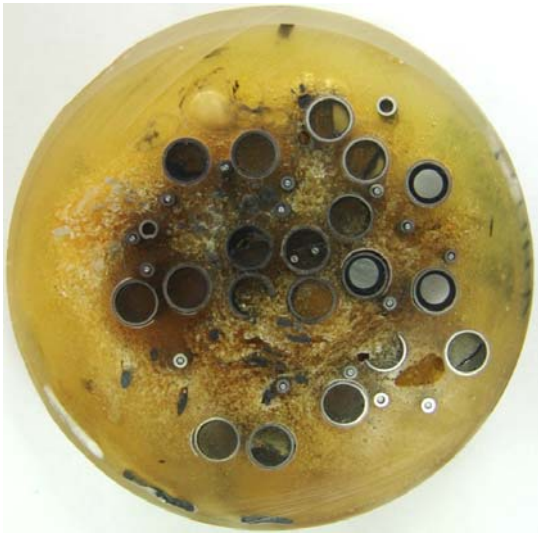

1400 mm

1500 mm

Fig. 4. Photos of the assembly cross-sections slabs within the range of Z ~ 1100…1500 mm elevations.

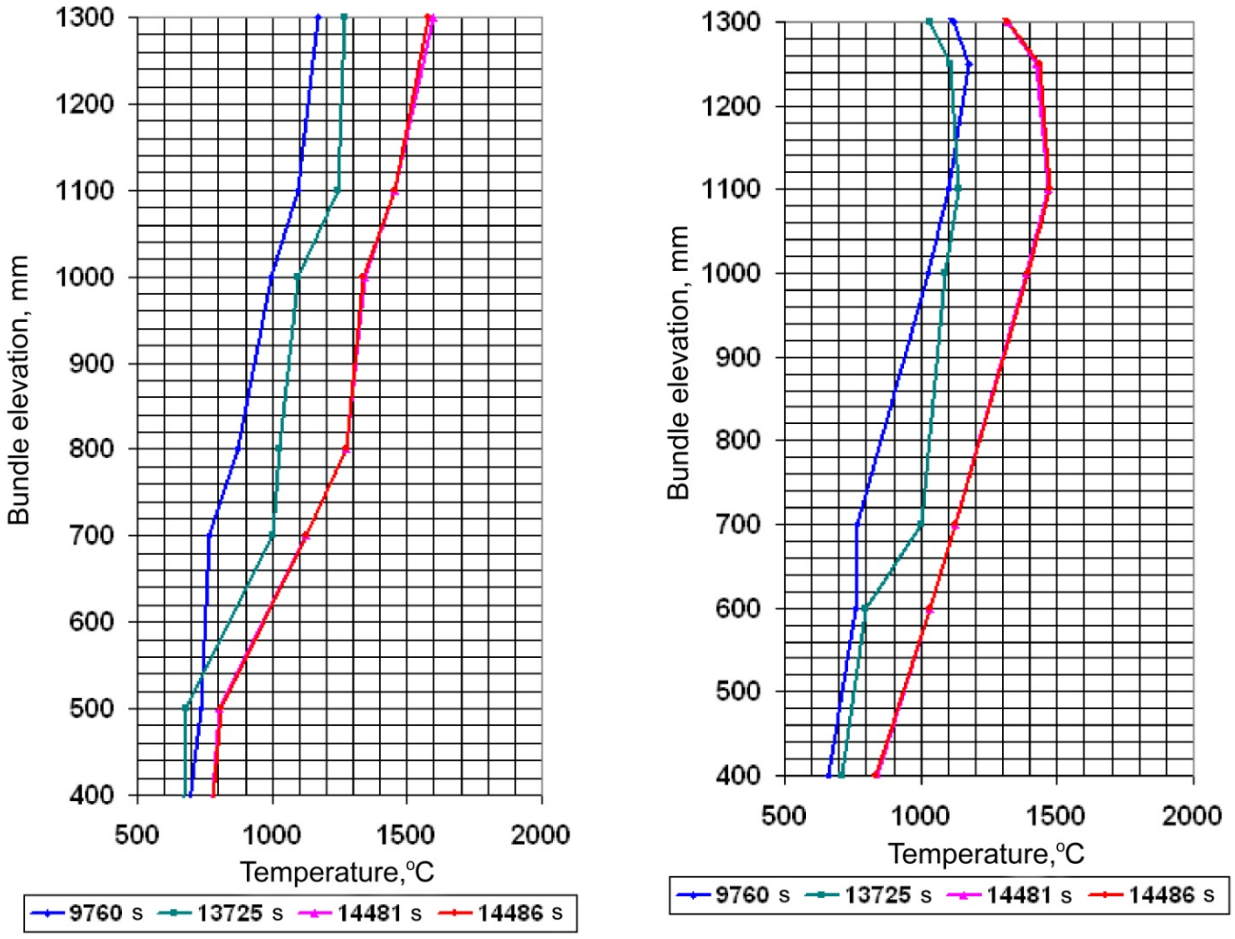

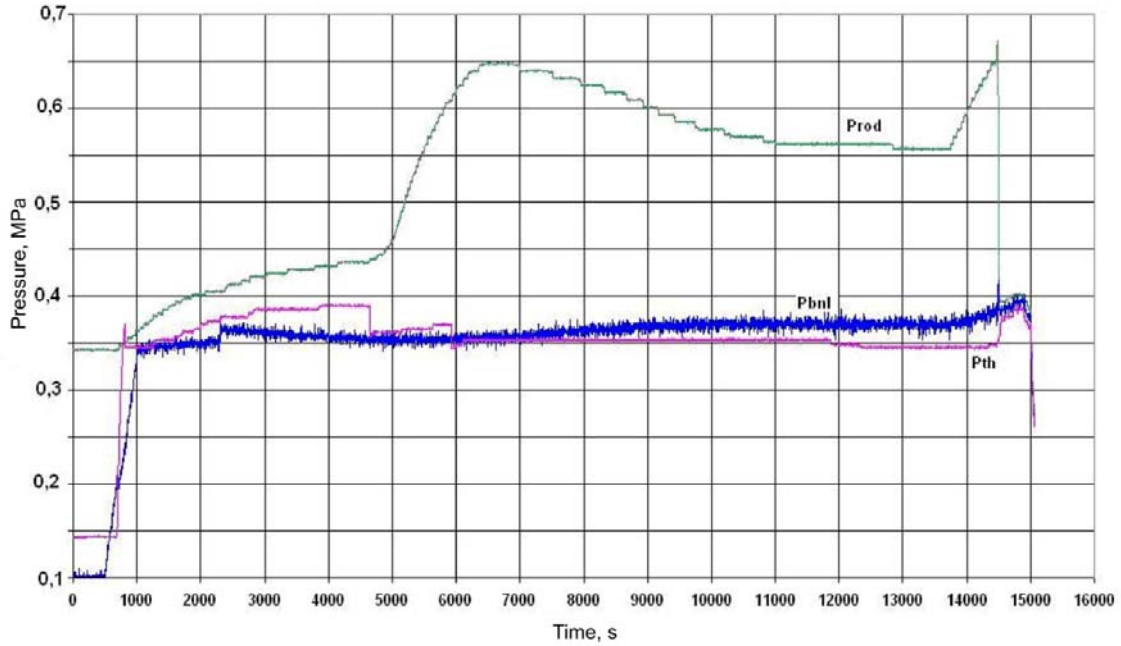

c

Fig. 5. Distribution of cladding temperatures of fuel rods of the second (a) and third (b) rows over the assembly height at the beginning of pre-oxidation stage (t = 9760 s), at the beginning of transient phase (t = 13725 s), at the moment of power switch off (t= 14486 s) and before flooding onset (t = 4481 s). Indications of pressure sensors in the model assembly (p_{bnl}), in fuel rods (p_{rod}) and cavity of thermal insulation (p_{th}) – c.

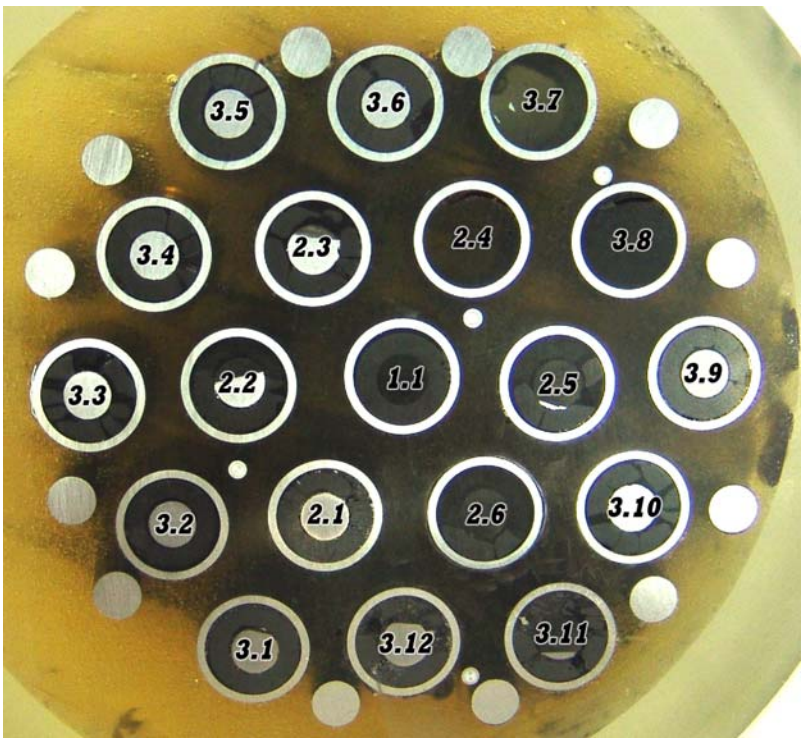

Fig. 6. Assembly cross-section at Z = 500 mm elevation (top view).

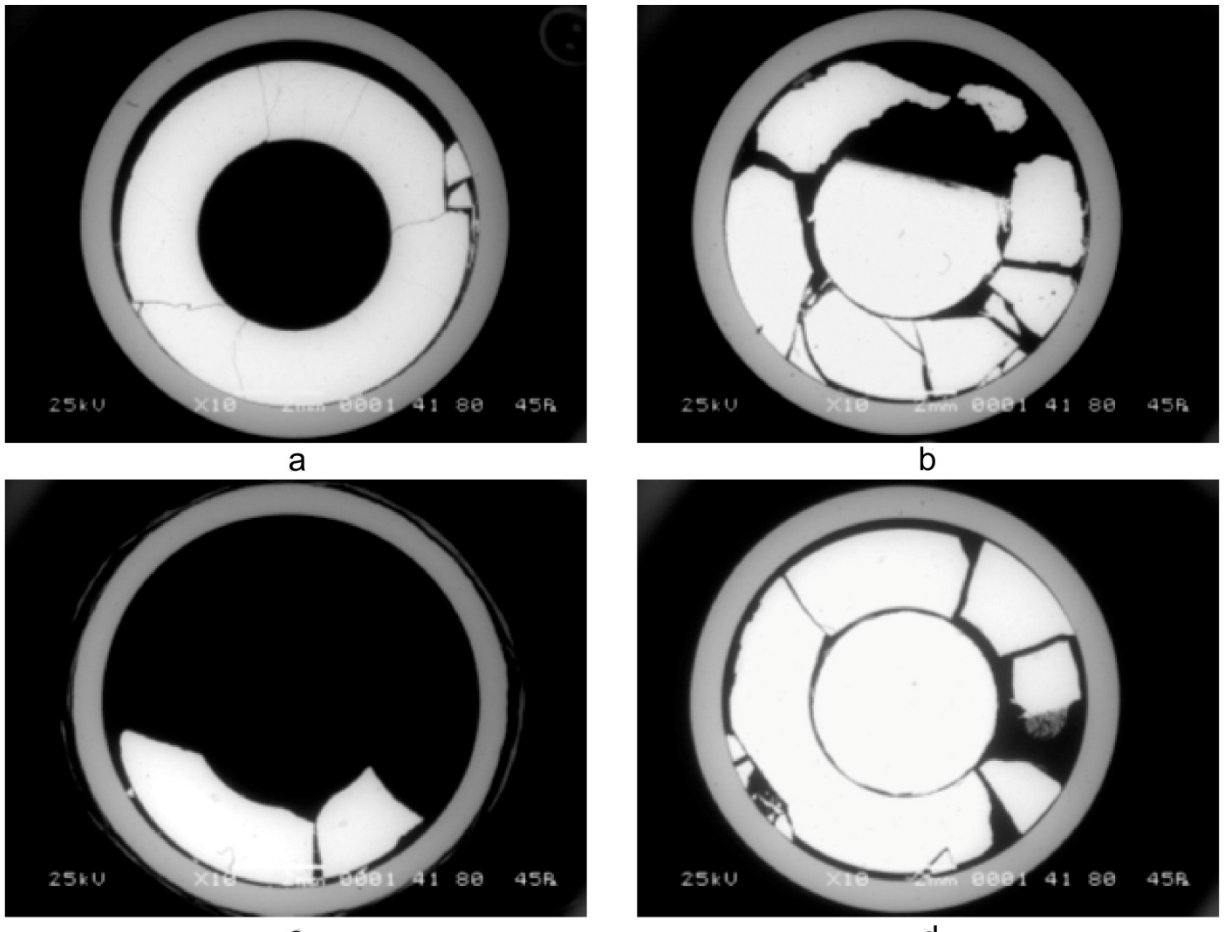

a b c d

Fig. 7. Macrographs of fuel rod simulators at Z = 500 mm elevation:
a – fuel rod 1.1; b – fuel rod 2.3; c – fuel rod 2.6; d – fuel rod 3.4.

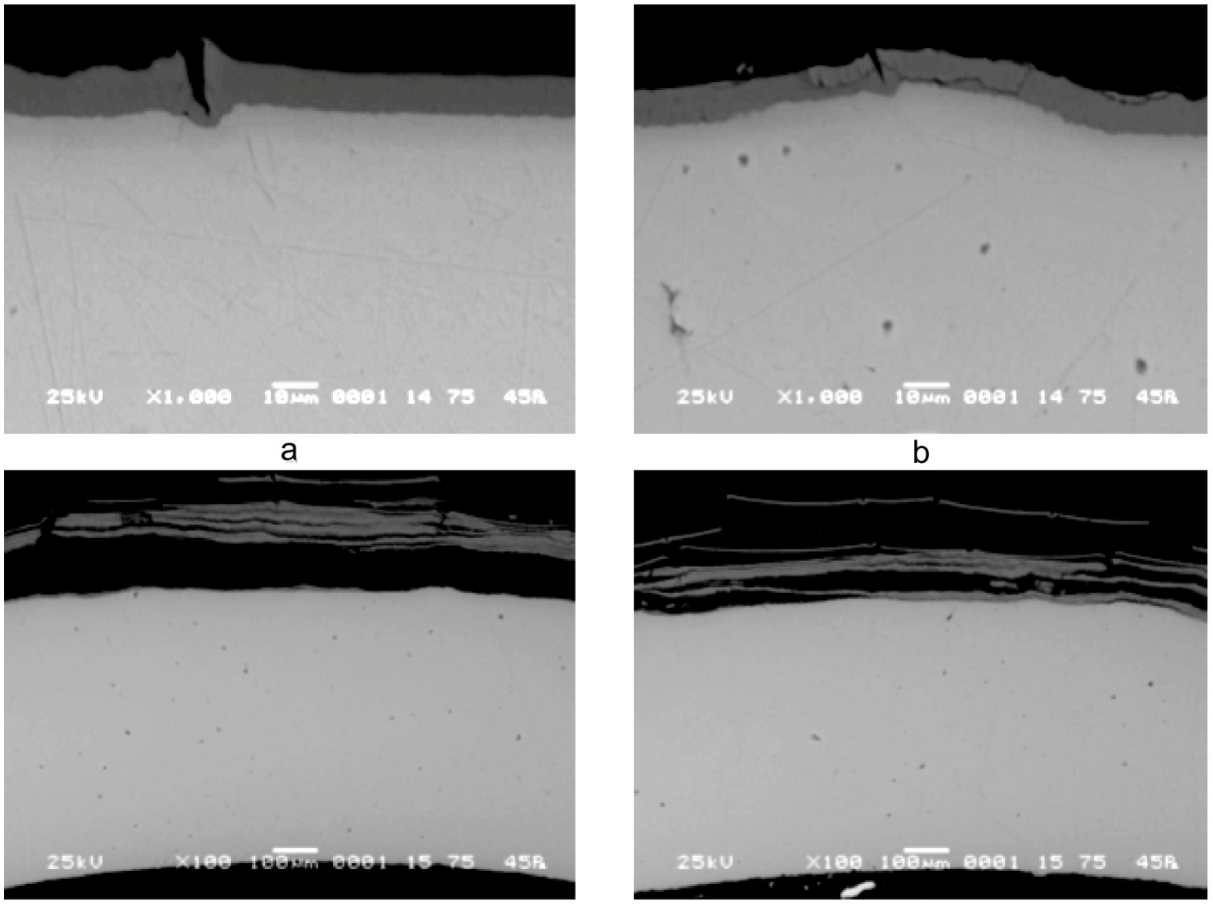

Fig. 8. Structure of oxide scale on fuel rod cladding surfaces at Z = 500 mm elevation: a – fuel rod 1.1; b – fuel rod 2.3; c – fuel rod 2.6; d – fuel rod 3.10.

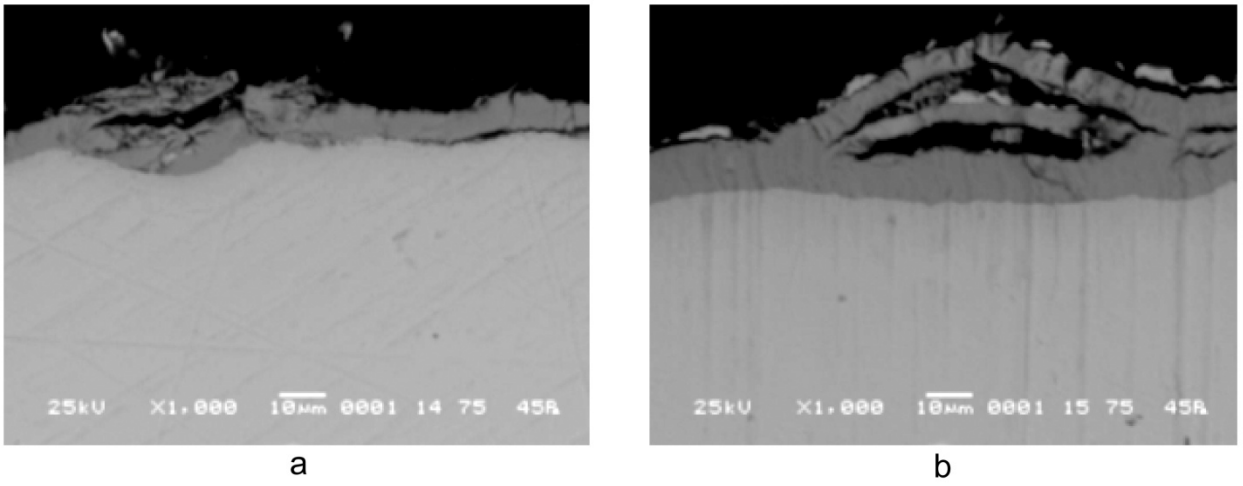

Fig. 9. Structure of oxide scale on periphery rod surfaces at Z = 500 mm elevation: a – located near fuel rod 3.6; b – located near fuel rod 3.12.

Fuel rod No.	1.1	2.1	2.2	2.3	2.4	2.5	2.6
Metal layer thickness, μm	656	644	652	667	657	642	620
Fuel rod No.	3.1	3.2	3.3	3.4	3.5	3.6	
Metal layer thickness, μm	659	659	673	673	670	670	
Fuel rod No.	3.7	3.8	3.9	3.10	3.11	3.12	
Metal layer thickness, μm	664	661	662	630	647	644	

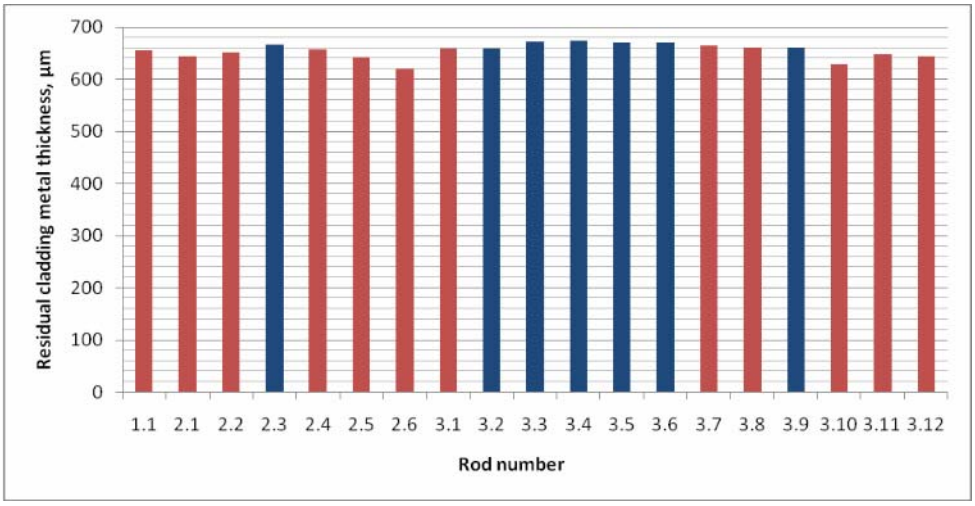

a

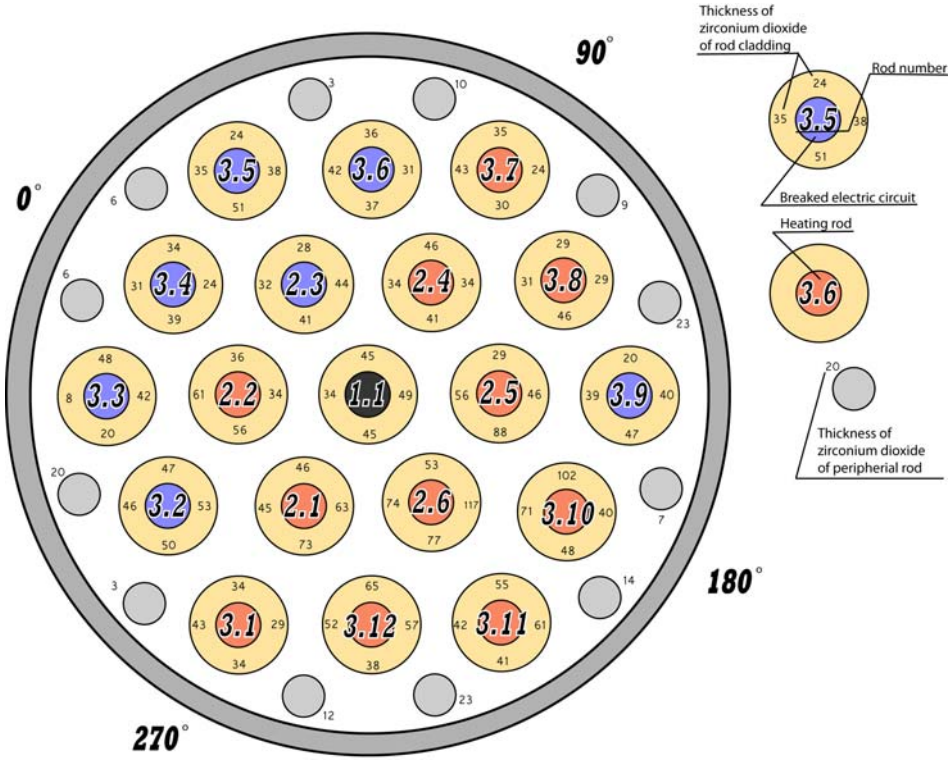

b

Fig. 10. a – Results of claddings residual metal layer thickness measurement at Z = 500 mm elevation ■ - heated fuel rod; ■ - fuel rod with failed heater), b – calculated values of oxide scale thickness on surfaces of claddings and periphery rods.

Fig. 11. Assembly cross-section at Z = 800 mm elevation (top view).

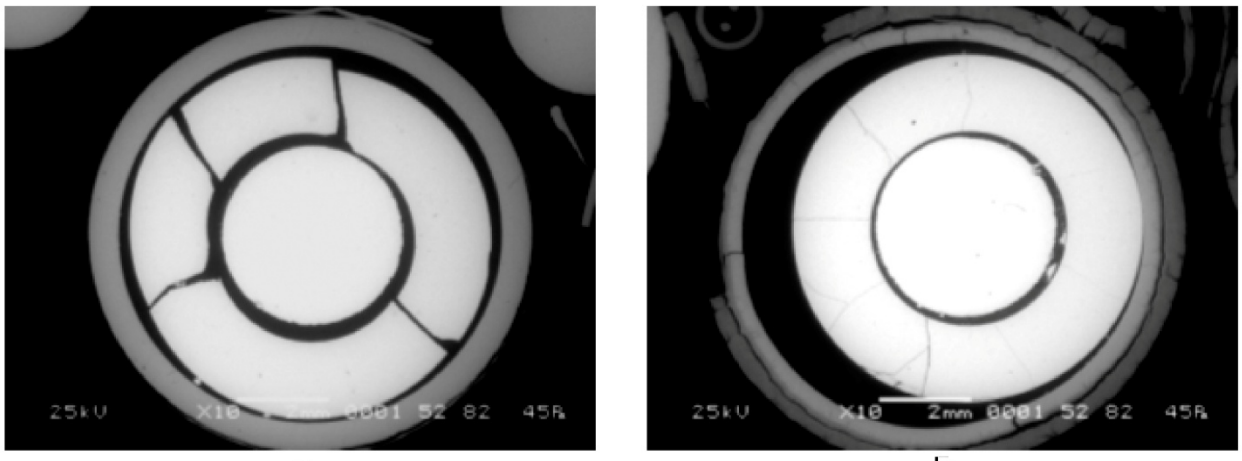

a b

Fig. 12. Macrographs of fuel rod simulators at Z = 800 mm elevation:
a – fuel rod 3.6; b – fuel rod 2.5.

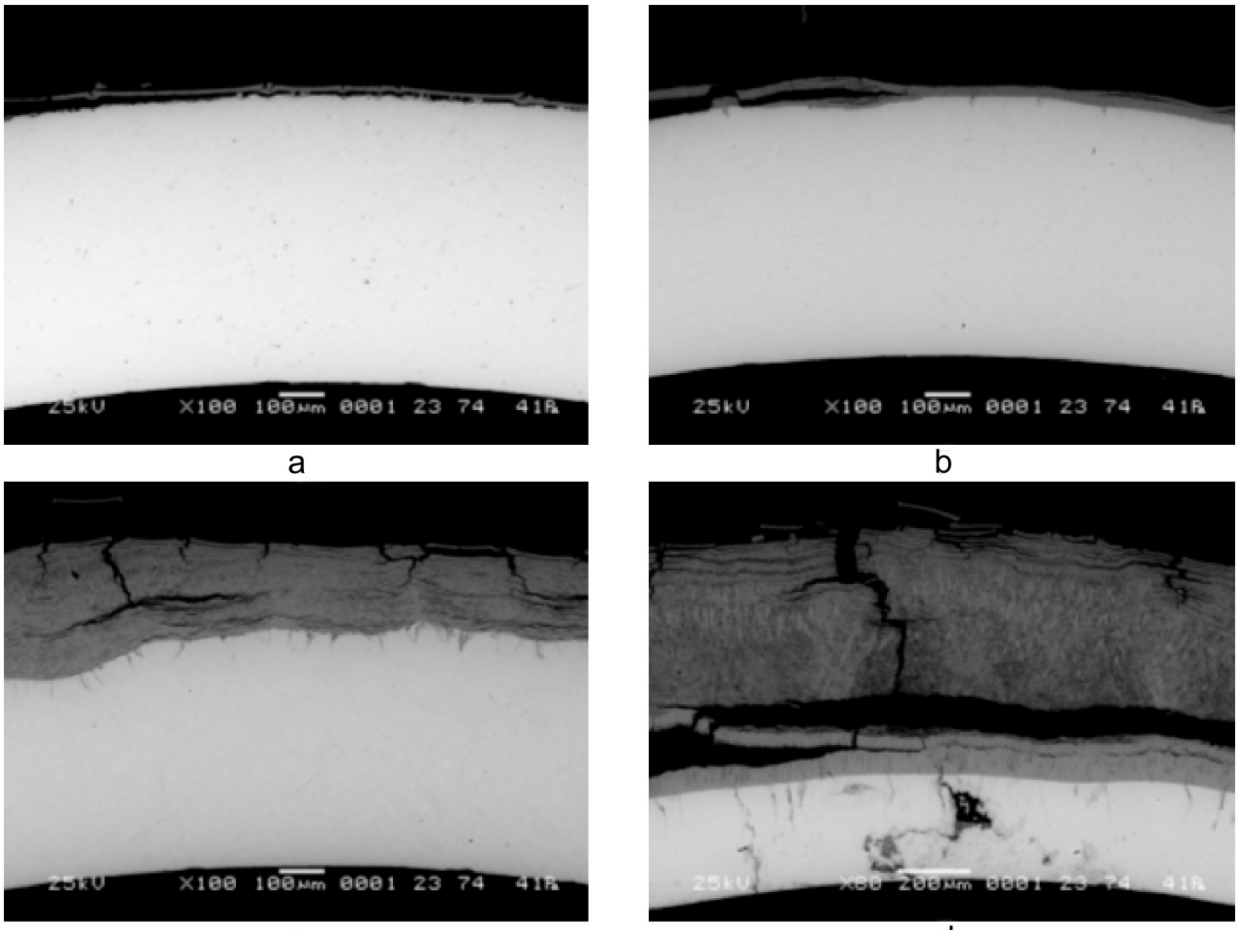

Fig. 13. Structure of fuel rod simulator claddings and their oxide scales at Z = 800 mm elevation:

a – fuel rod 3.6; b – fuel rod 3.2; c – fuel rod 2.2, d – fuel rod 2.5.

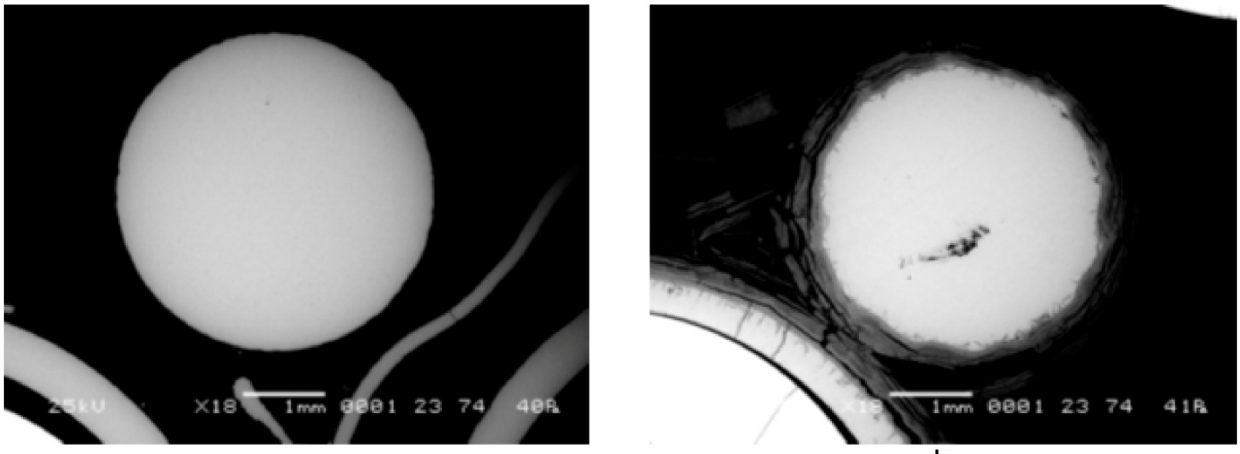

a b

Fig. 14. Macrographs of periphery rods at Z = 800 mm elevation:
a – located near fuel rod 3.6; b – located near fuel rod 3.11.

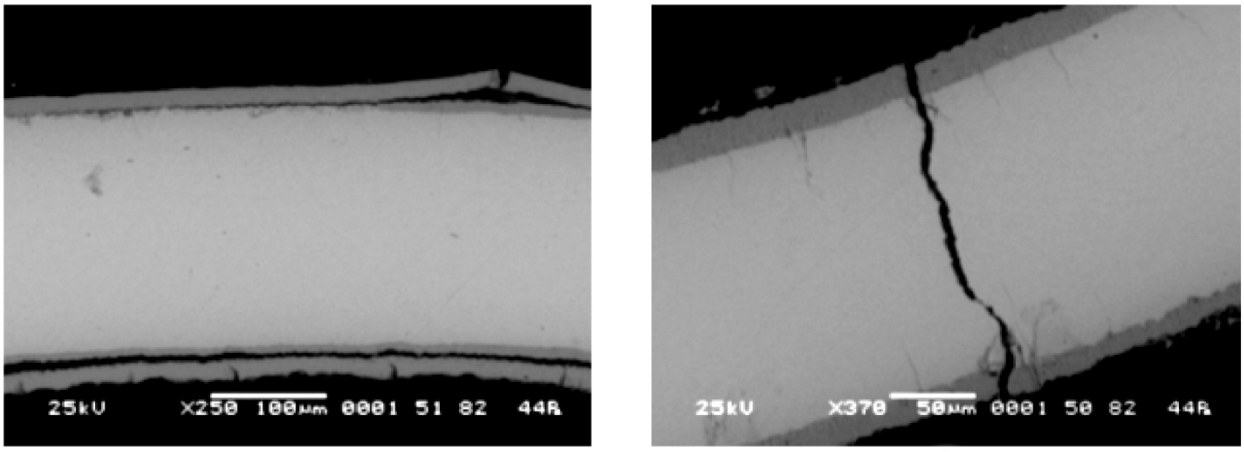

a b

Fig. 15. Oxidation state of spacer grid at Z = 800 mm elevation.

Fuel rod No.	1.1	2.1	2.2	2.3	2.4	2.5	3.1	3.2
Metal layer thickness, μm	571	560	473	559	426	324	384	568
Fuel rod No.	3.3	3.4	3.5	3.6	3.7	3.8	3.9	3.11
Metal layer thickness, μm	603	613	635	627	568	575	460	418

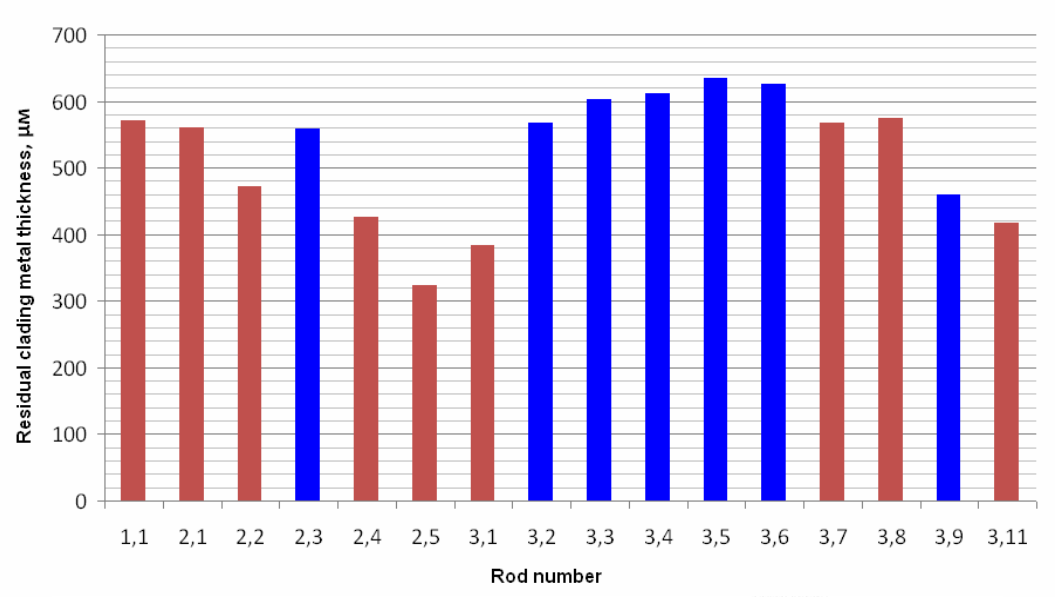

a

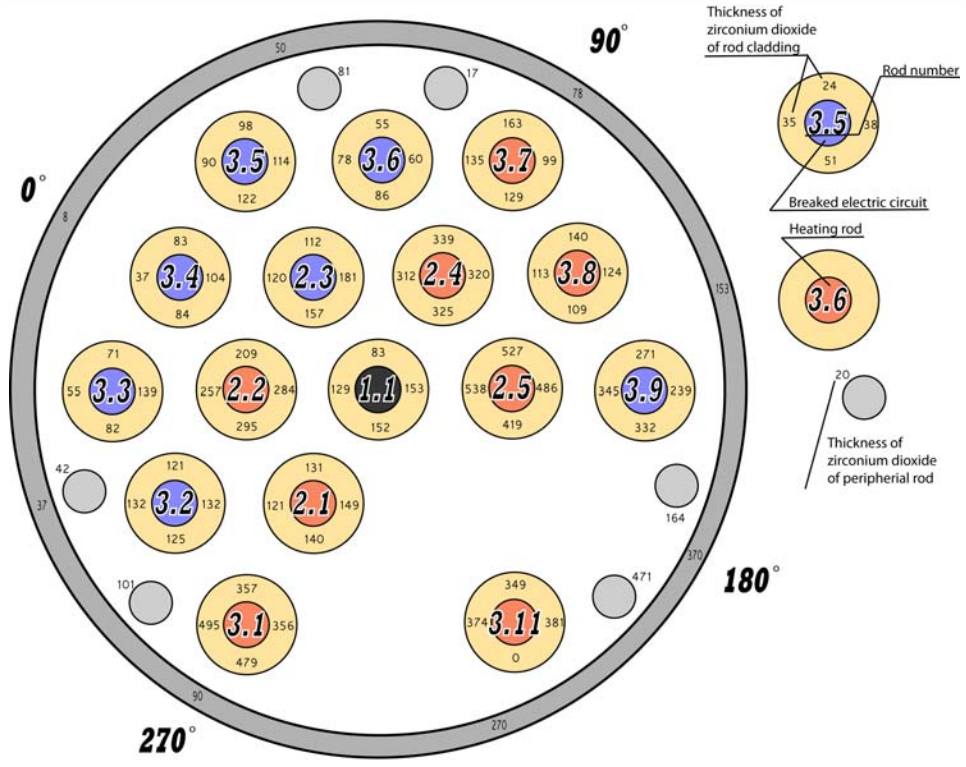

b

Fig. 16. a – Results of claddings residual metal layer thickness measurement at Z = 800 mm elevation (- heated fuel rod; - fuel rod with failed heater), b – calculated values of oxide scale thickness on surfaces of claddings, shroud and periphery rods.

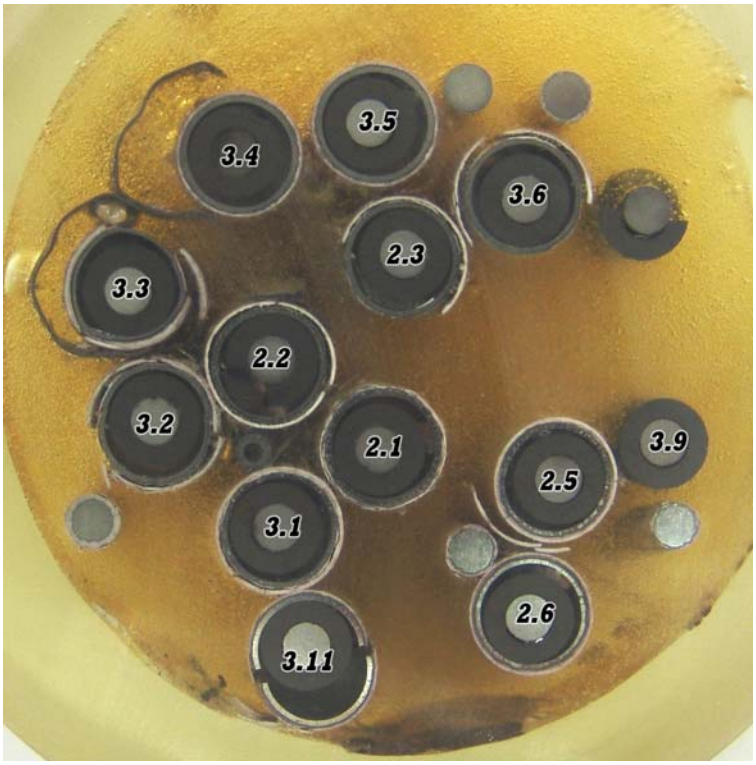

Fig. 17. Assembly cross-section at Z = 1000 mm elevation (top view).

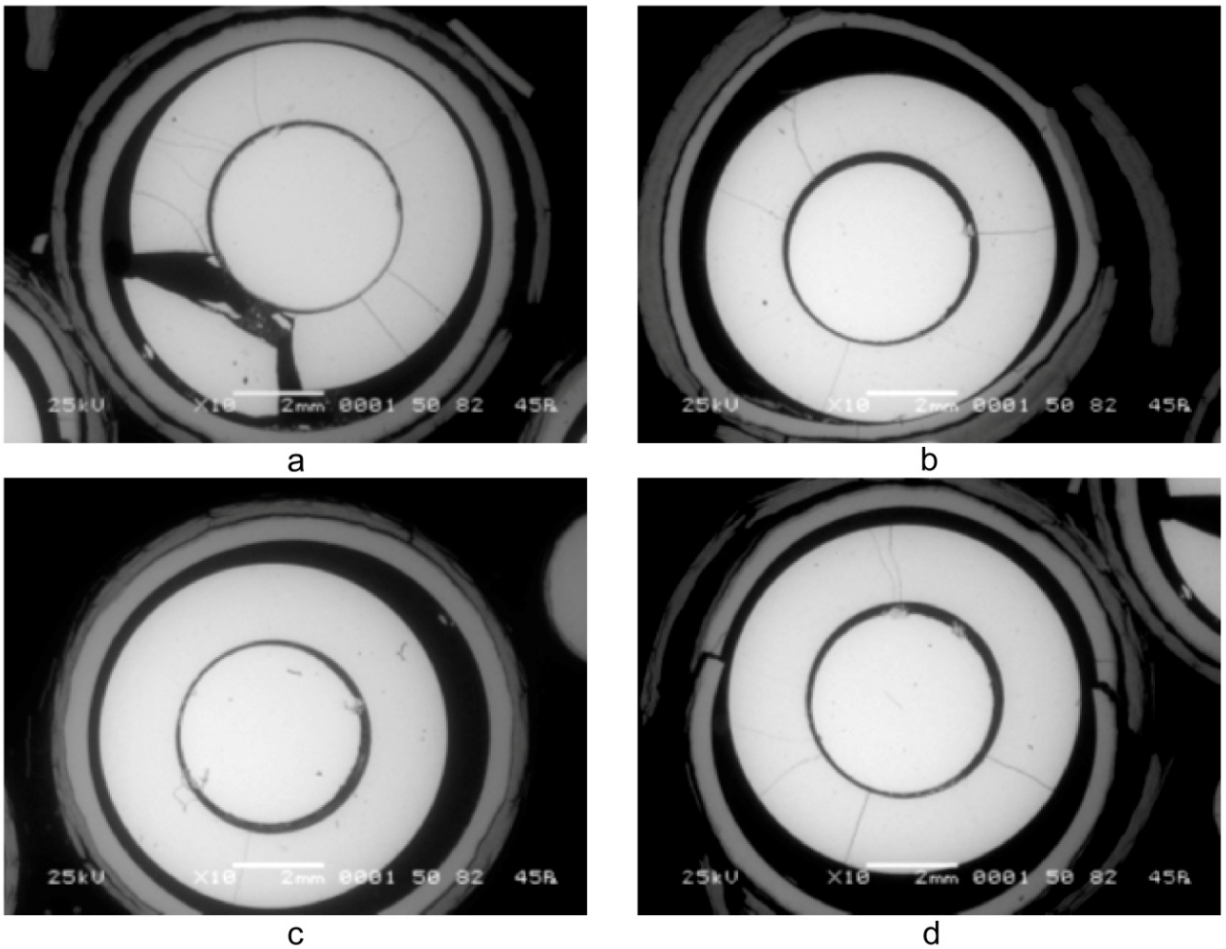

Fig. 18. Macrographs of fuel rod simulators at Z = 1000 mm elevation:
a – fuel rod 2.2; b – fuel rod 3.3; c – fuel rod 3.5; d – fuel rod 3.2.

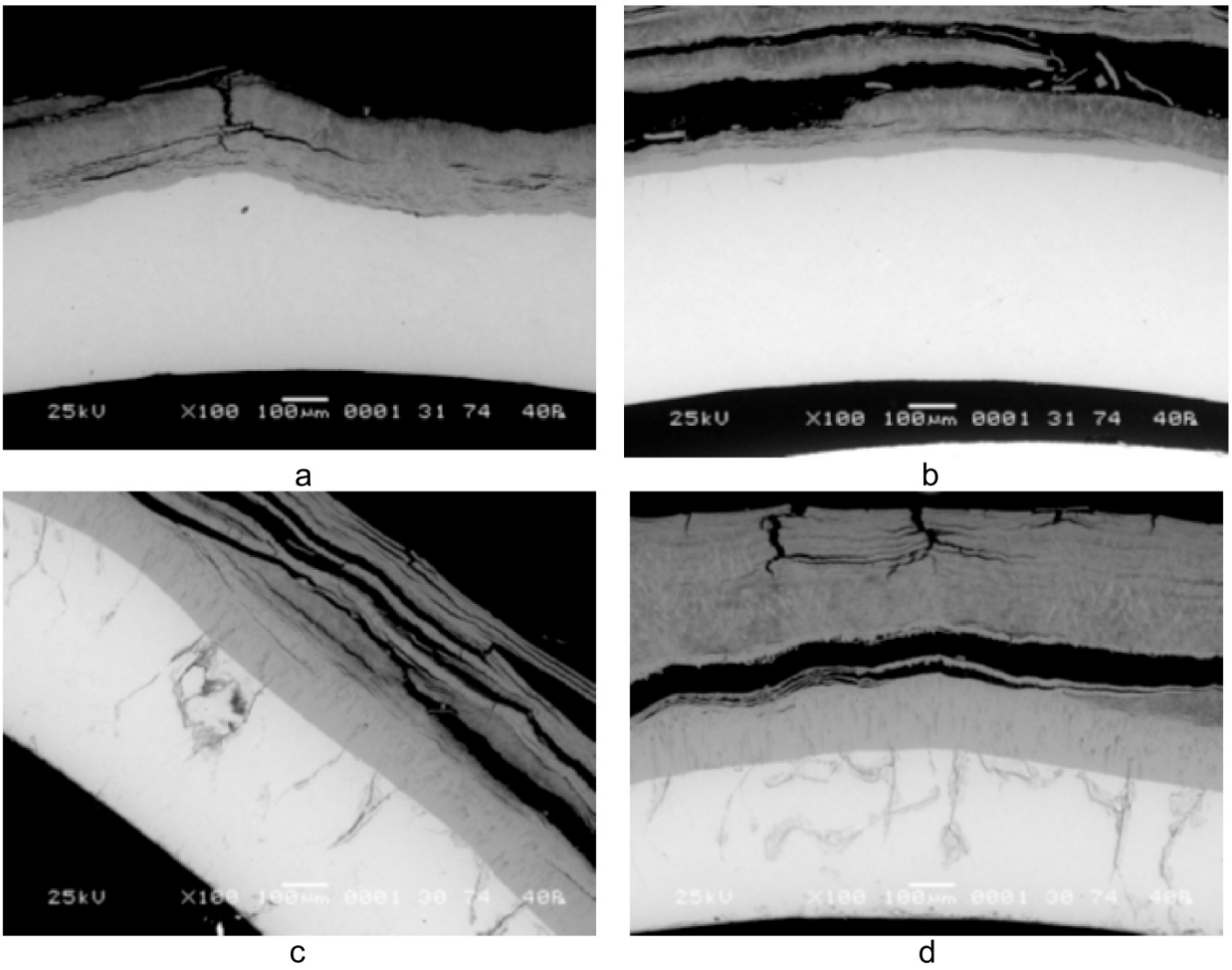

Fig. 19. Structure of fuel rod simulator claddings and their oxide scales at Z = 1000 mm elevation:
a – fuel rod 3.6; b – fuel rod 2.3; c – fuel rod 2.1, d – fuel rod 2.5.

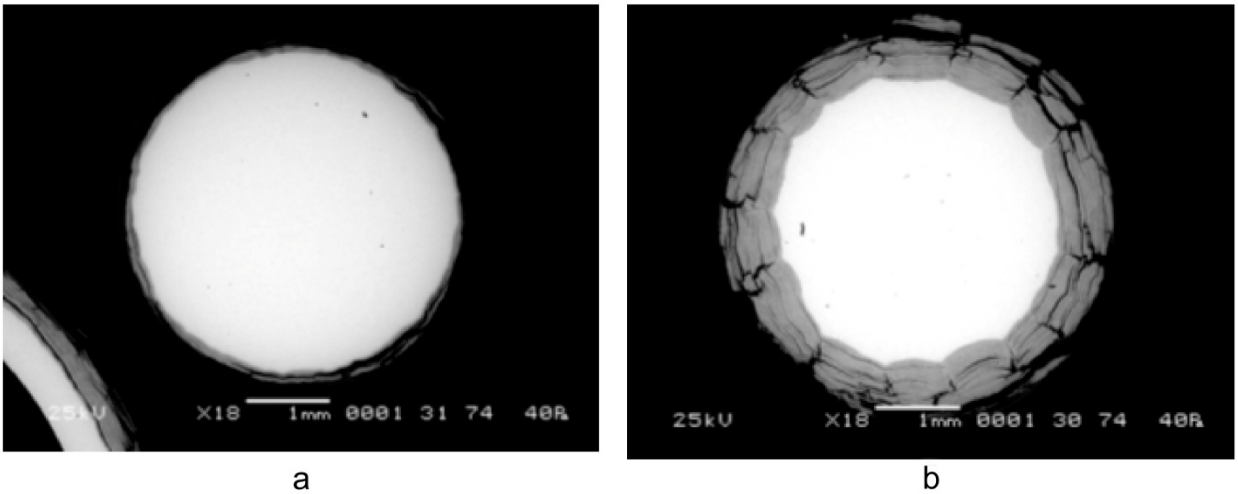

Fig. 20. Macrographs of periphery rods at Z = 1000 mm elevation:
a – located near fuel rod 3.5; b – located near fuel rod 3.2.

Fuel rod No.	2.1	2.2	2.3	2.5	2.6	3.1
Metal layer thickness, μm	461	414	460	332	343	349
Fuel rod No.	3.2	3.3	3.4	3.5	3.6	3.11
Metal layer thickness, μm	364	301	459	441	417	421

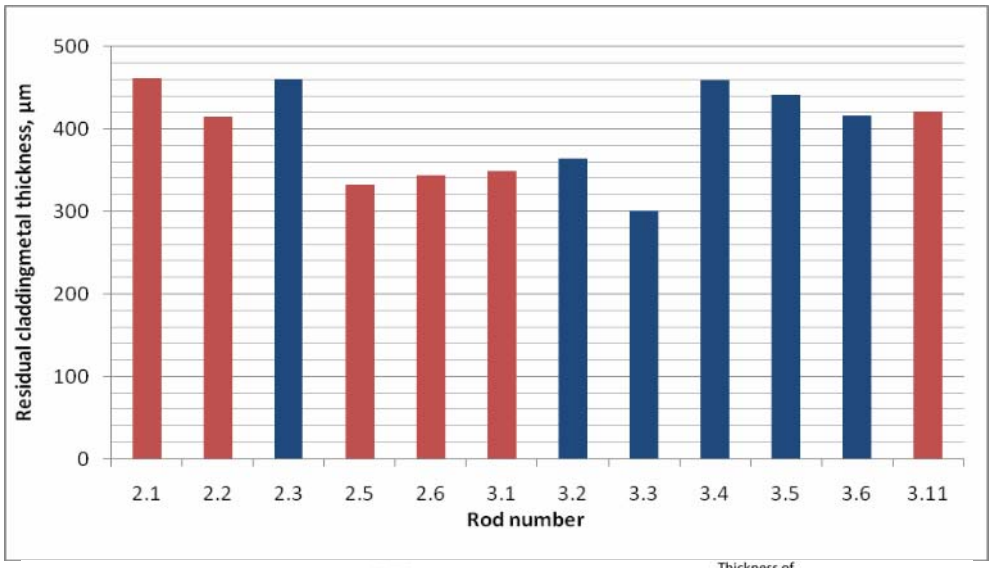

a

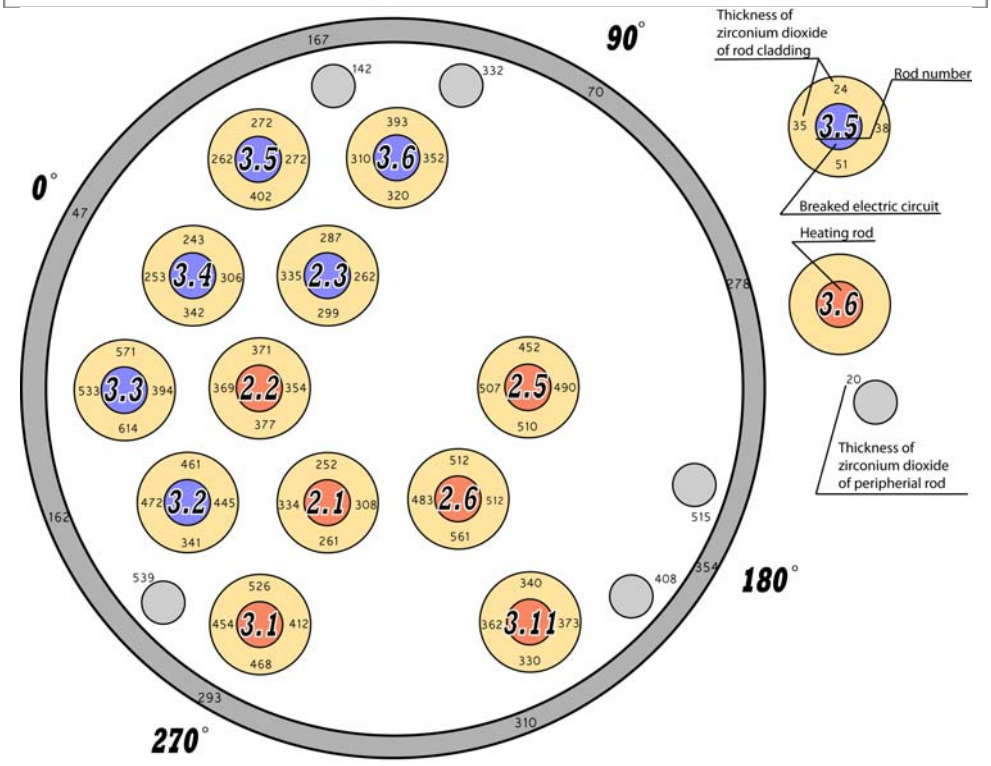

b

Fig. 21. a – Results of claddings residual metal layer thickness measurement at Z = 1000 mm elevation (- heated fuel rod, - fuel rod with failed heater), b – calculated values of oxide scale thickness on surfaces of claddings, shroud and periphery rods.

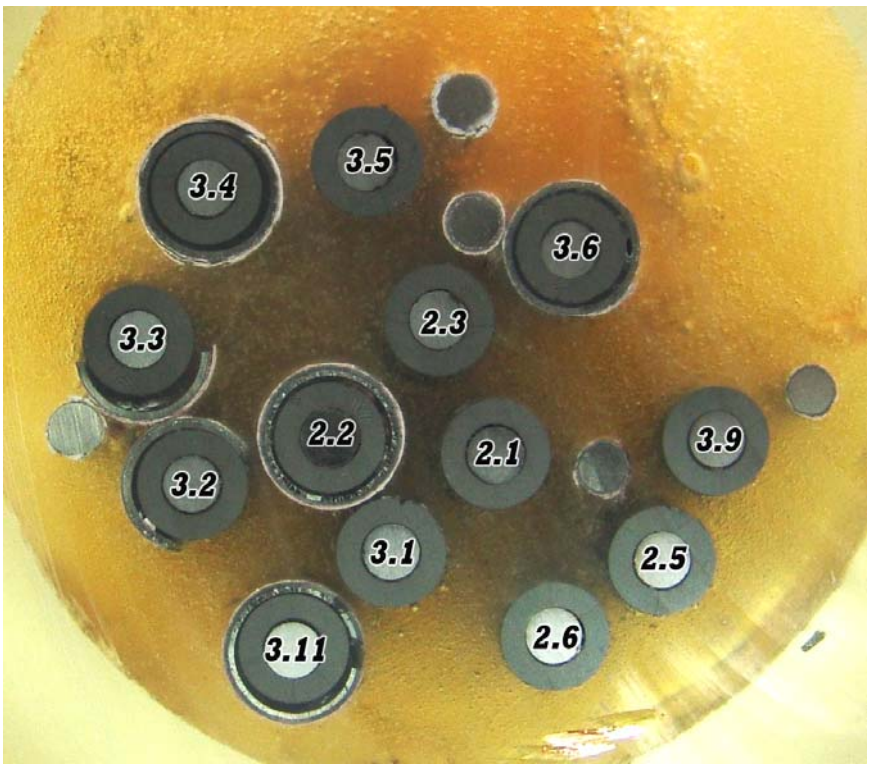

Fig. 22. Assembly cross-section at Z = 1200 mm elevation (top view).

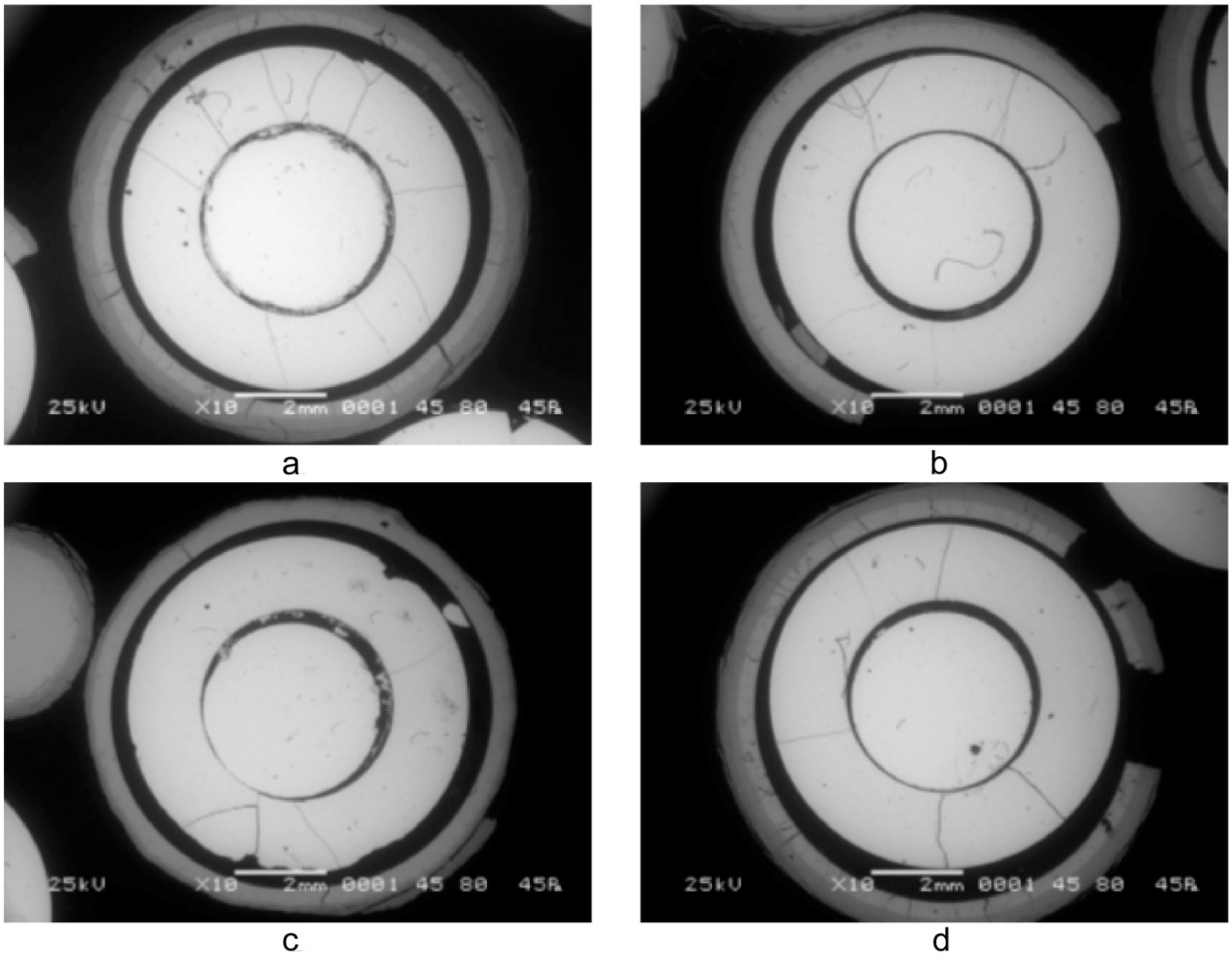

Fig. 23. Macrographs of fuel rod simulators at Z = 1200 mm elevation:
a – fuel rod 2.2; b – fuel rod 3.2; c – fuel rod 3.6; d – fuel rod 3.11.

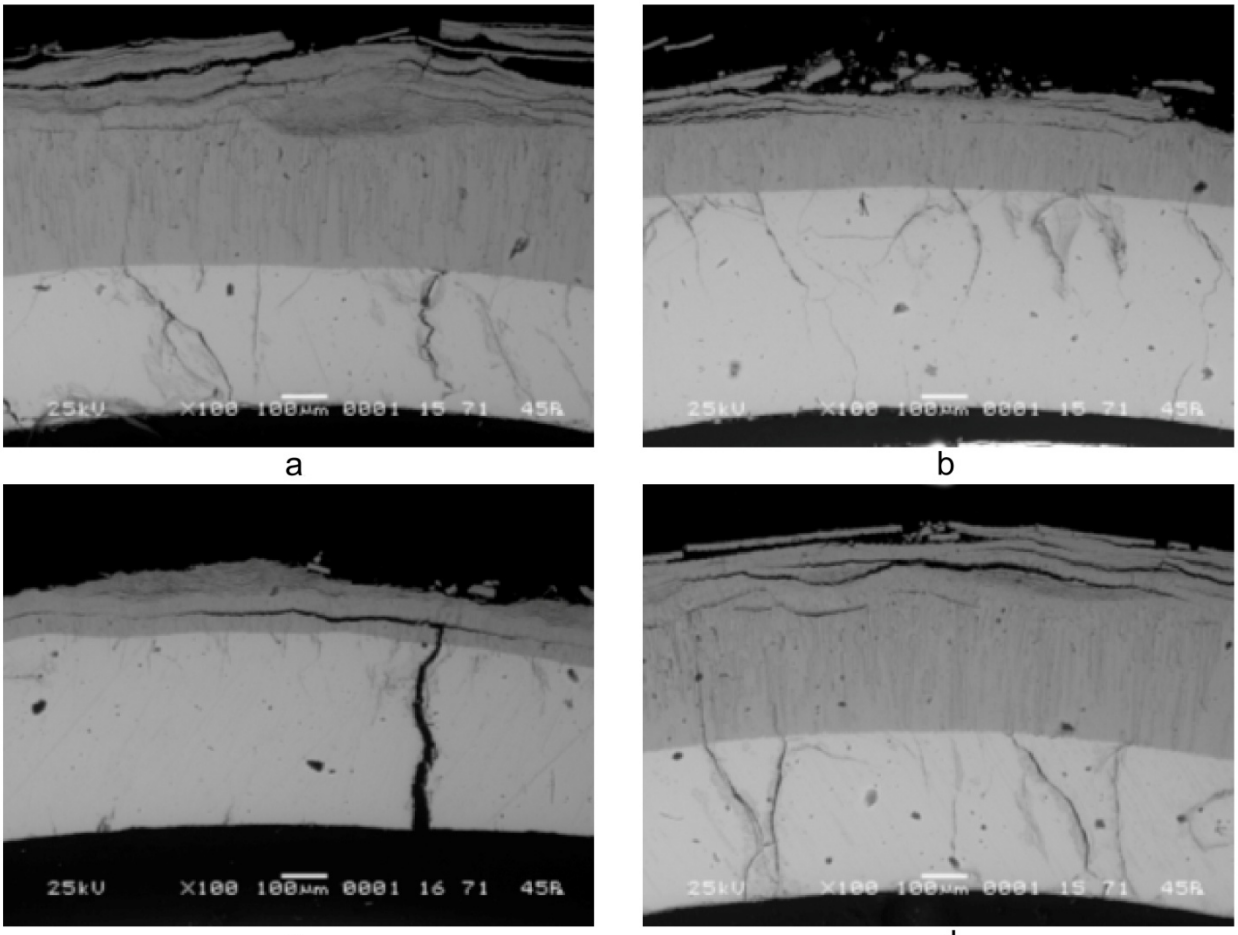

a b

c d

Fig. 24. Structure of fuel rod simulator claddings and their oxide scales at Z = 1200 mm elevation:

a – fuel rod 2.2; b – fuel rod 3.2; c – fuel rod 3.6, d – fuel rod 3.11.

.

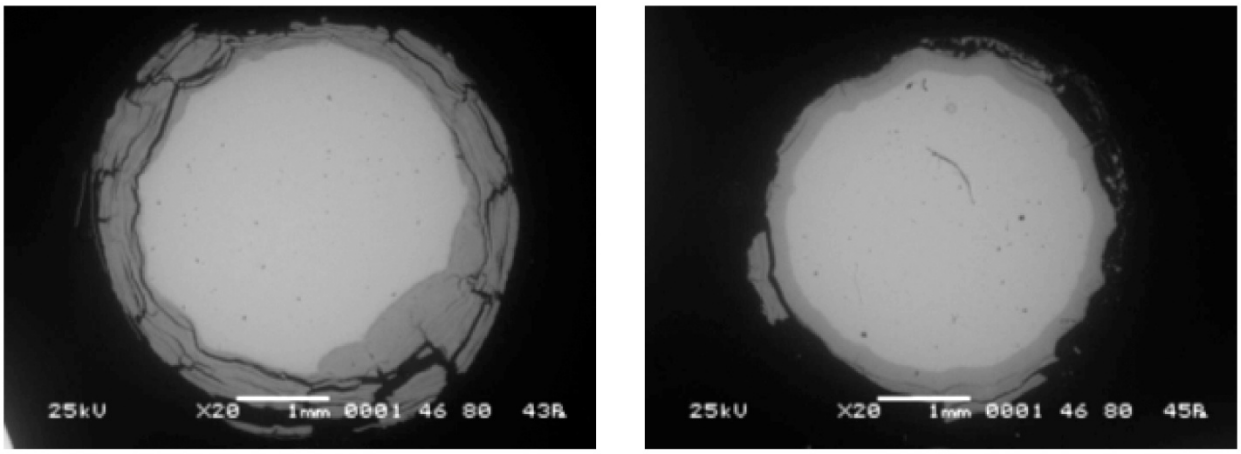

a b

Fig. 25. Macrographs of periphery rods at Z = 1200 mm elevation:

a – located near fuel rod 3.5; b – located near fuel rod 3.3.

Fuel rod No.	2.2	3.2	3.3	3.4	3.6	3.11
Metal layer thickness, μm	325	523	435	423	378	354

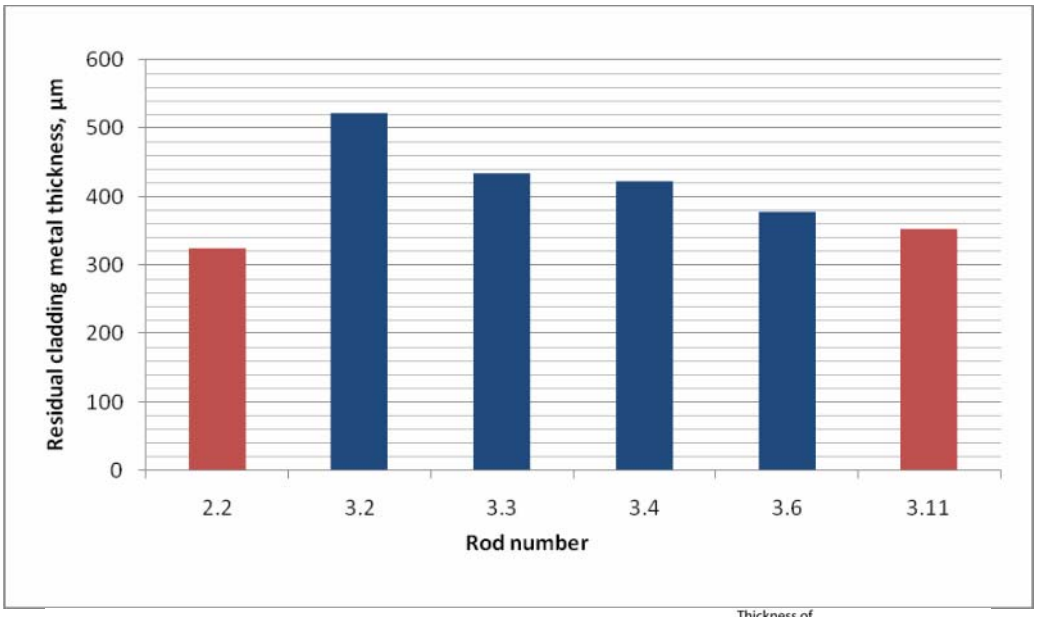

a

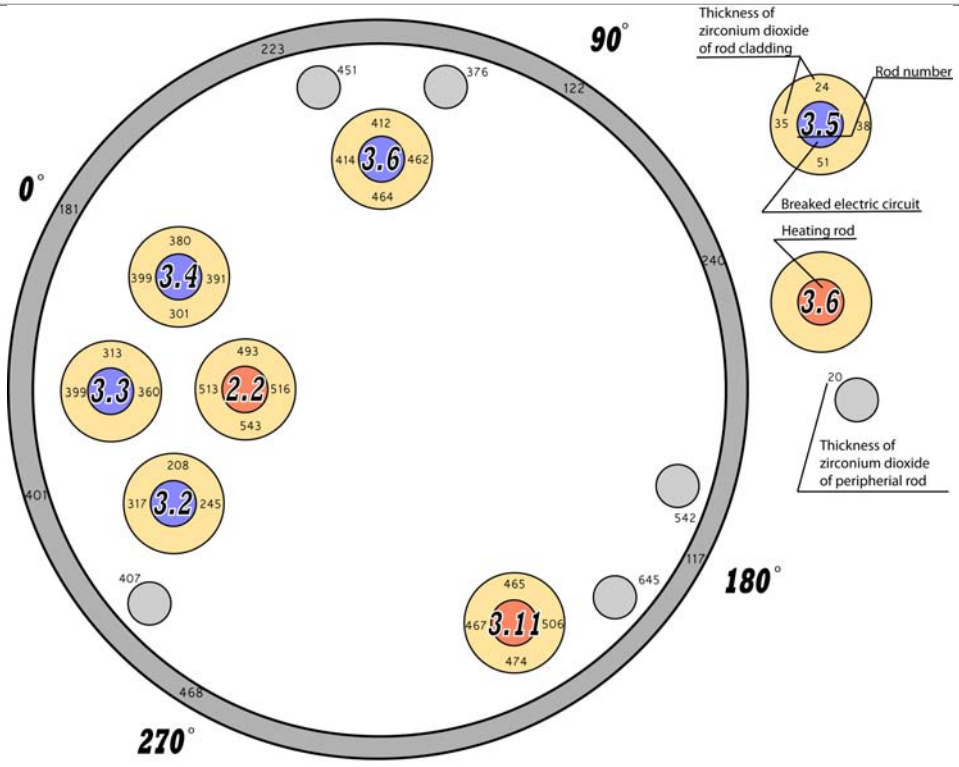

b

Fig. 26. a – Results of claddings residual metal layer thickness measurement at Z = 1200 mm elevation - heated fuel rod - fuel rod with failed heater), b – calculated values of oxide scale thickness on surfaces of claddings, shroud and periphery rods.

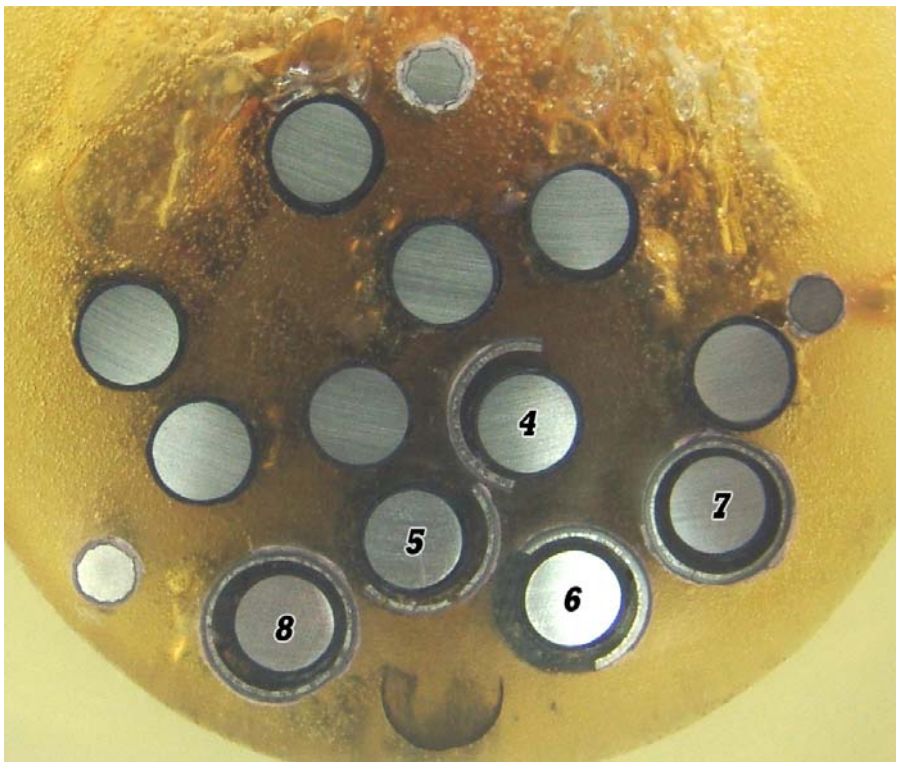

Fig. 27. Assembly cross-section at Z = 1300 mm elevation (top view).

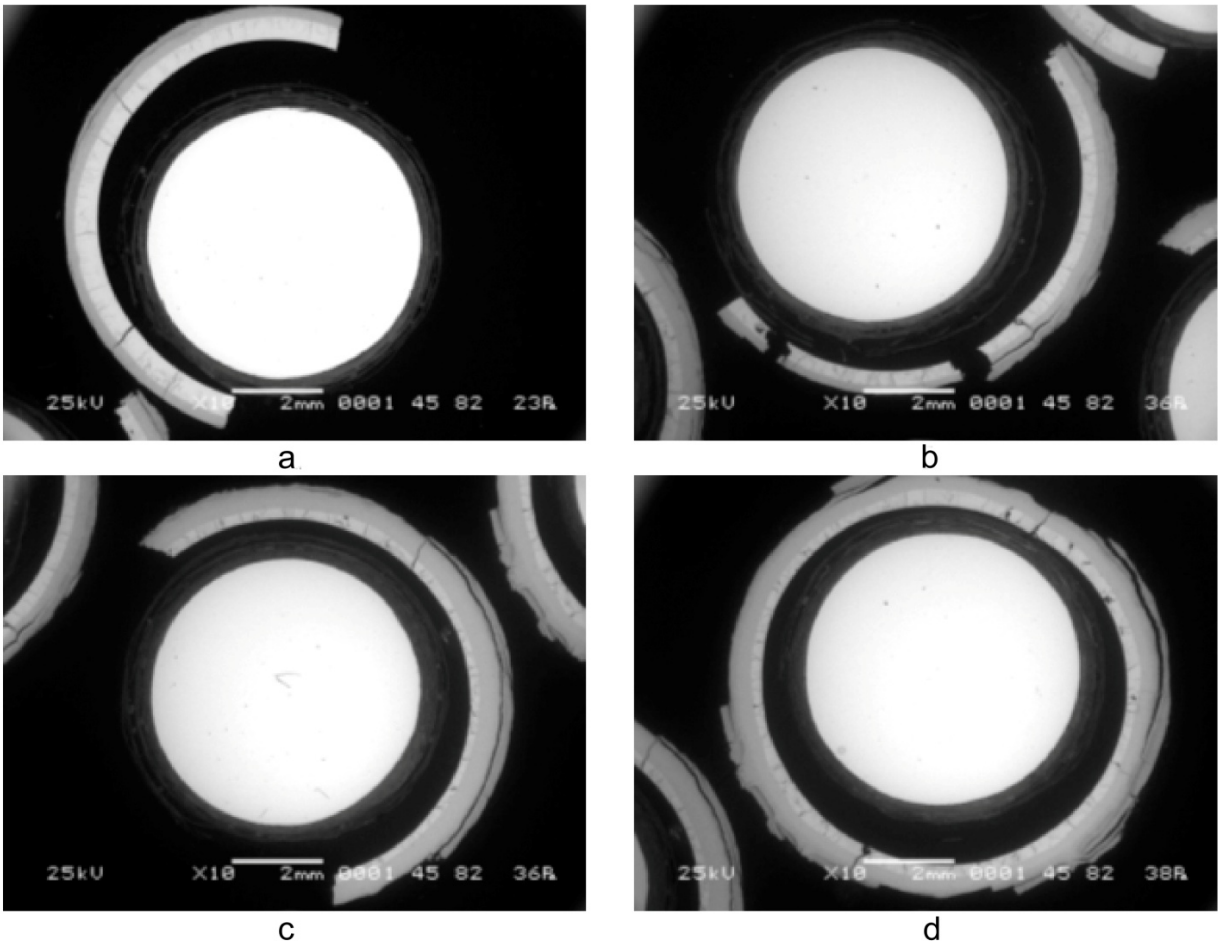

a b c d

Fig. 28. Macrographs of fuel rod simulators at Z = 1300 mm elevation:
a – fuel rod 4; b – fuel rod 5; c – fuel rod 6; d – fuel rod 7.

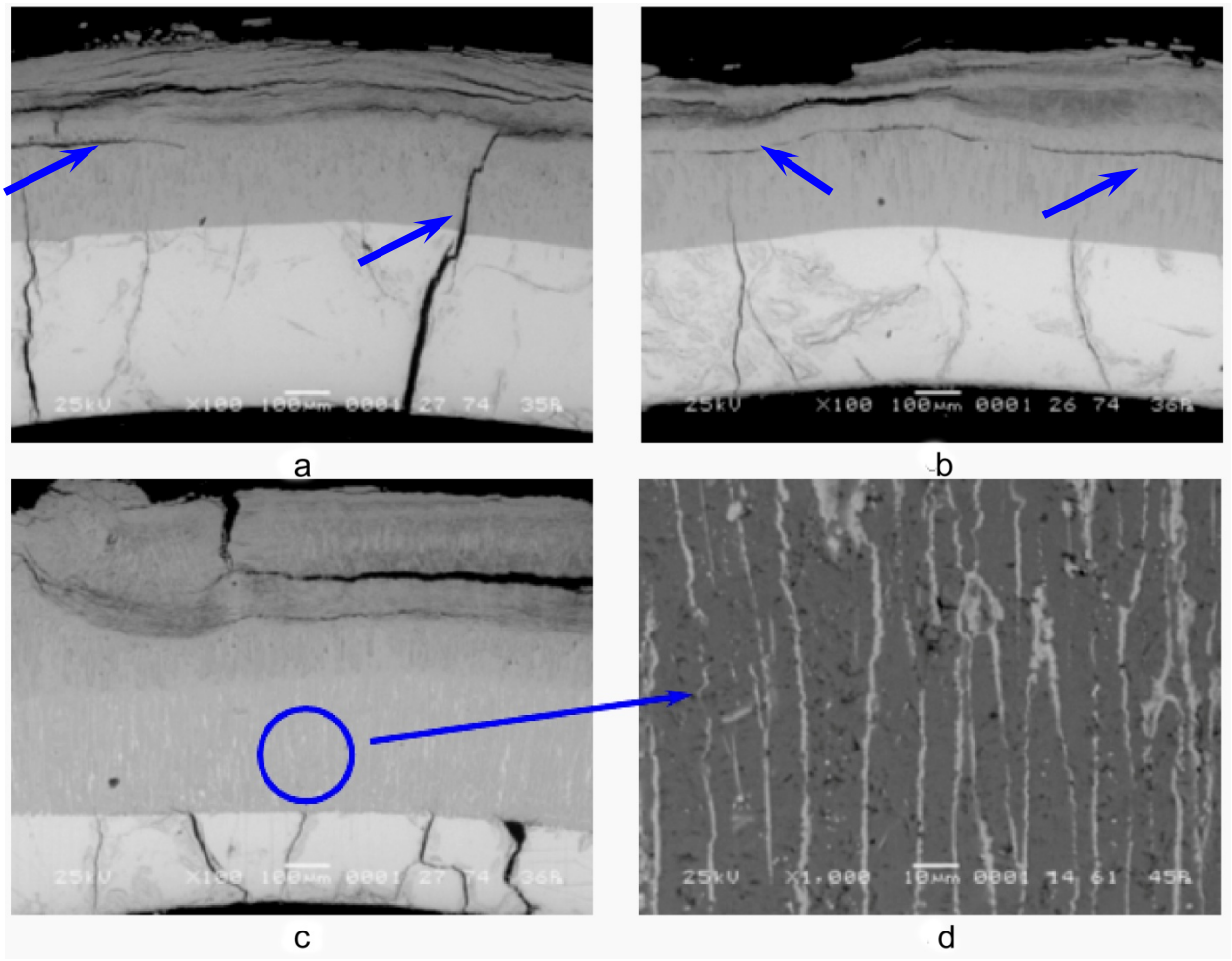

Fig. 29. Structure of fuel rod simulator claddings and their oxide scales at Z = 1300 mm elevation:

a – fuel rod 4; b – fuel rod 5; c – fuel rod 7, a – fuel rod 7 x1000.

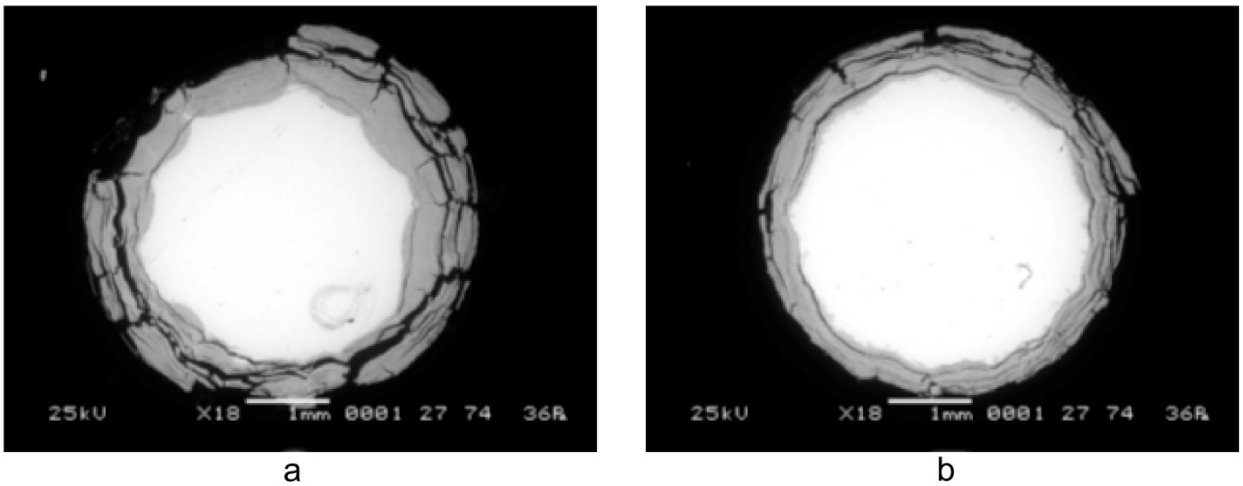

Fig. 30. Macrographs of periphery rods at Z = 1300 mm elevation:

a – located in Fig. 27 on the top; b – located in Fig. 27 on the left.

Fuel rod No.	4	5	6	7	8
Metal layer thickness, μm	518	320	221	284	311

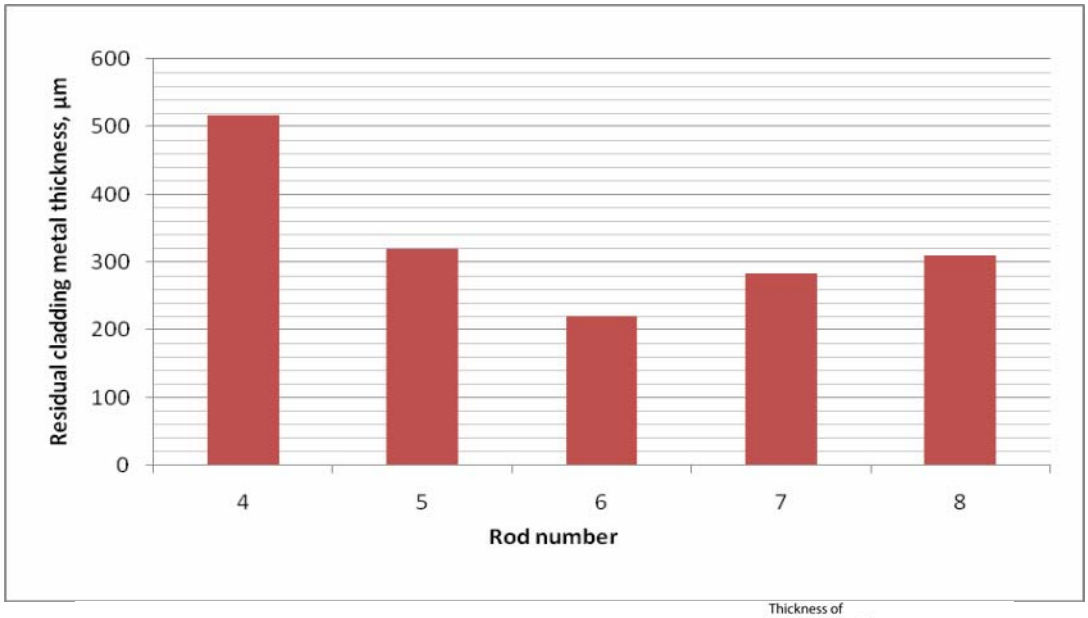

a

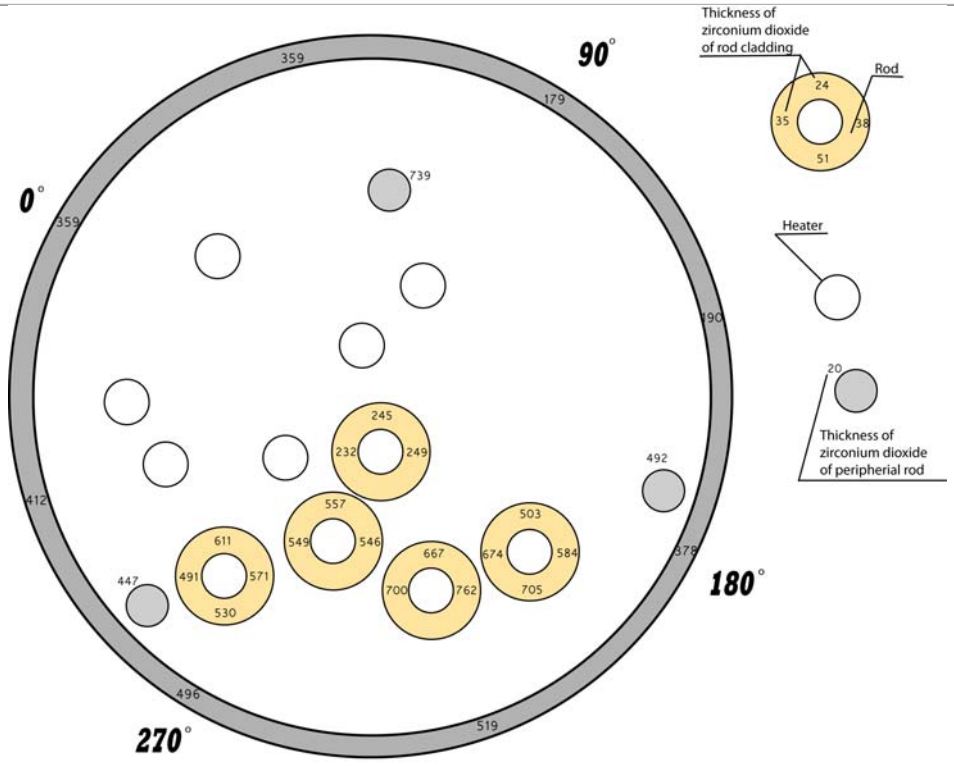

b

Fig. 31. a – Results of claddings residual metal layer thickness measurement at Z = 1300 mm elevation, b – calculated values of oxide scale thickness on surfaces of claddings, shroud and periphery rods.

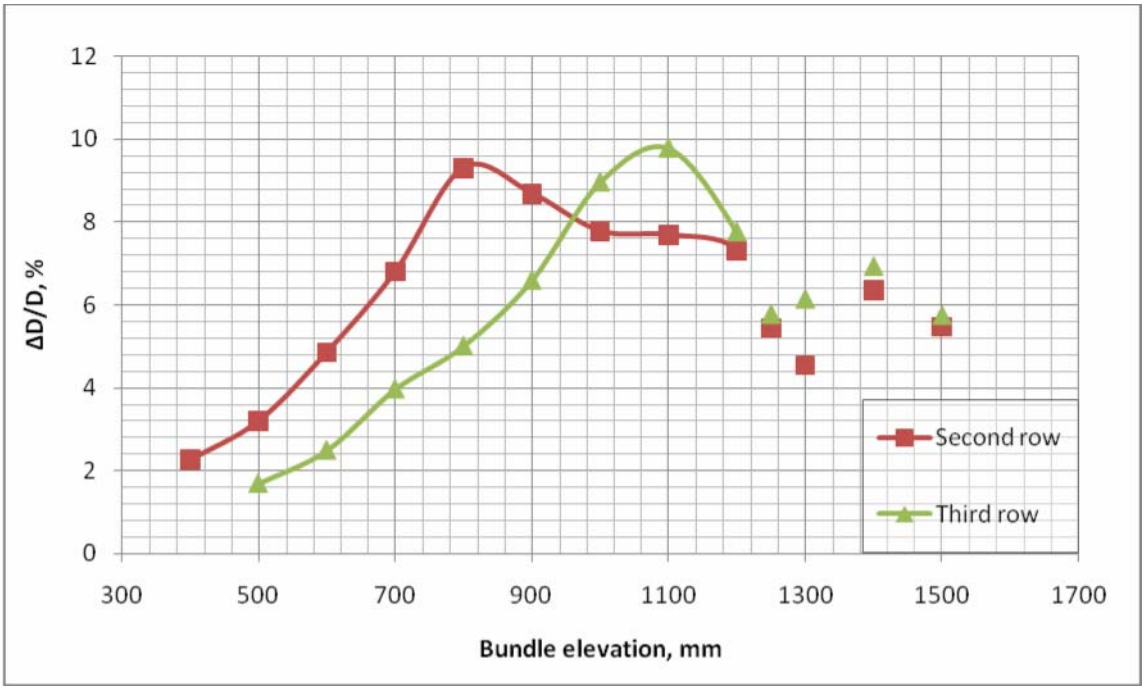

Fig. 32. Distribution of circumferential deformation of fuel rods over the assembly height.

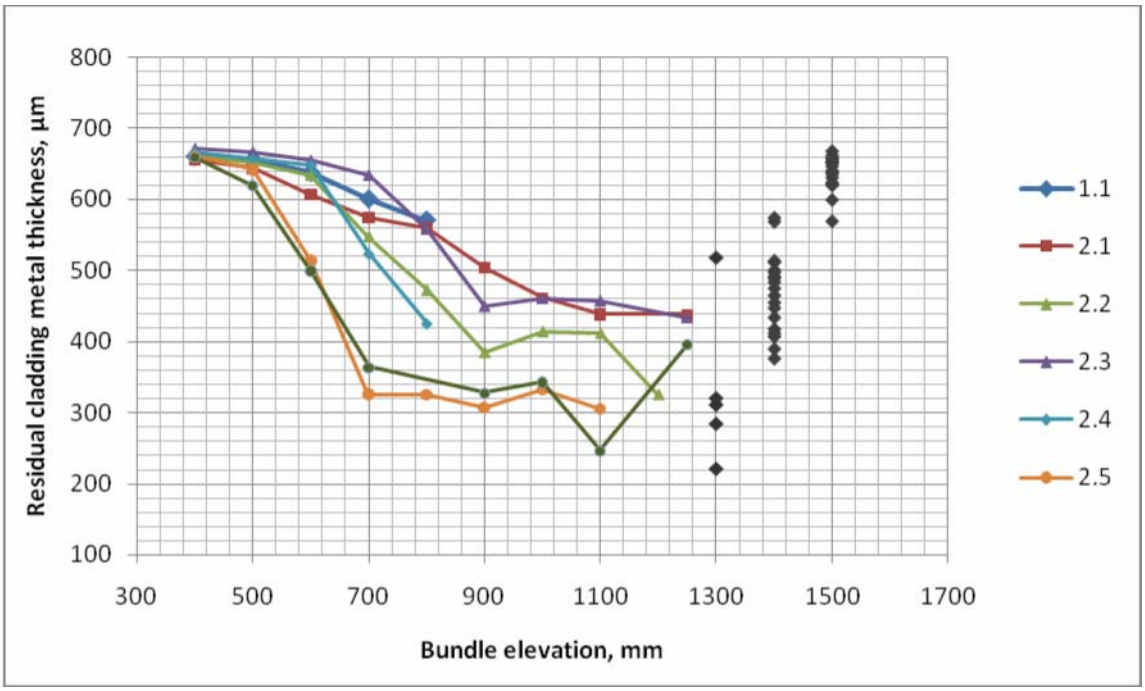

Fig. 33. Distribution of thickness of the remained metal part of claddings of fuel rods in the second row over the assembly height.

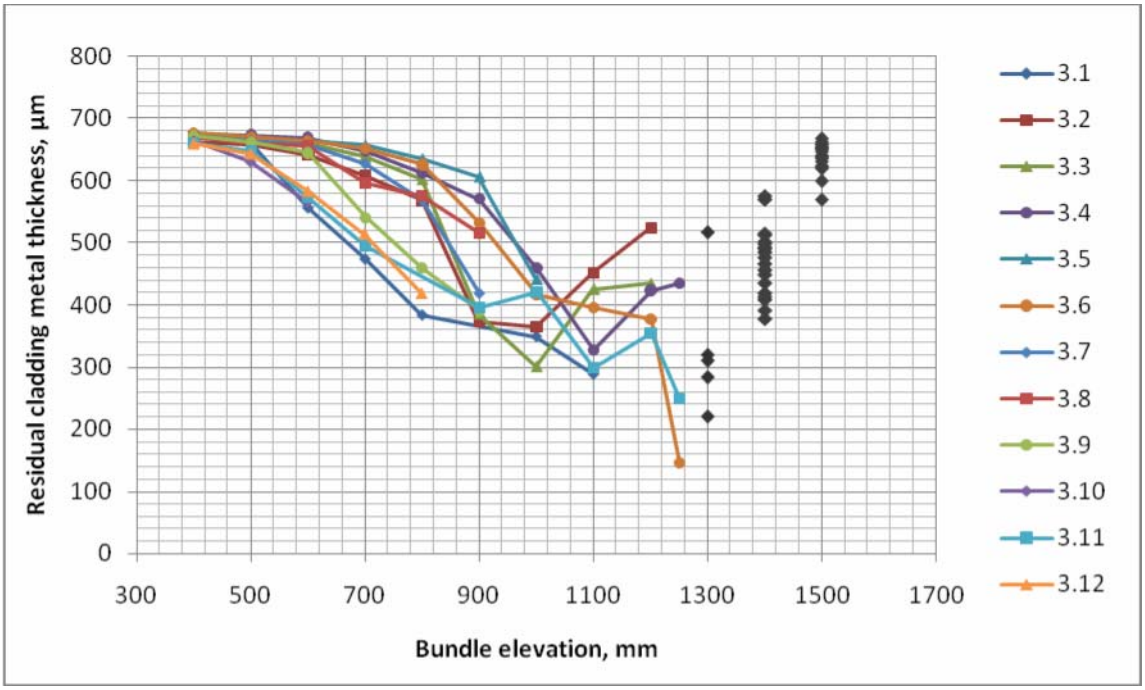

Fig. 34. Distribution of thickness of the remained metal part of claddings of fuel rods in the third row over the assembly height.

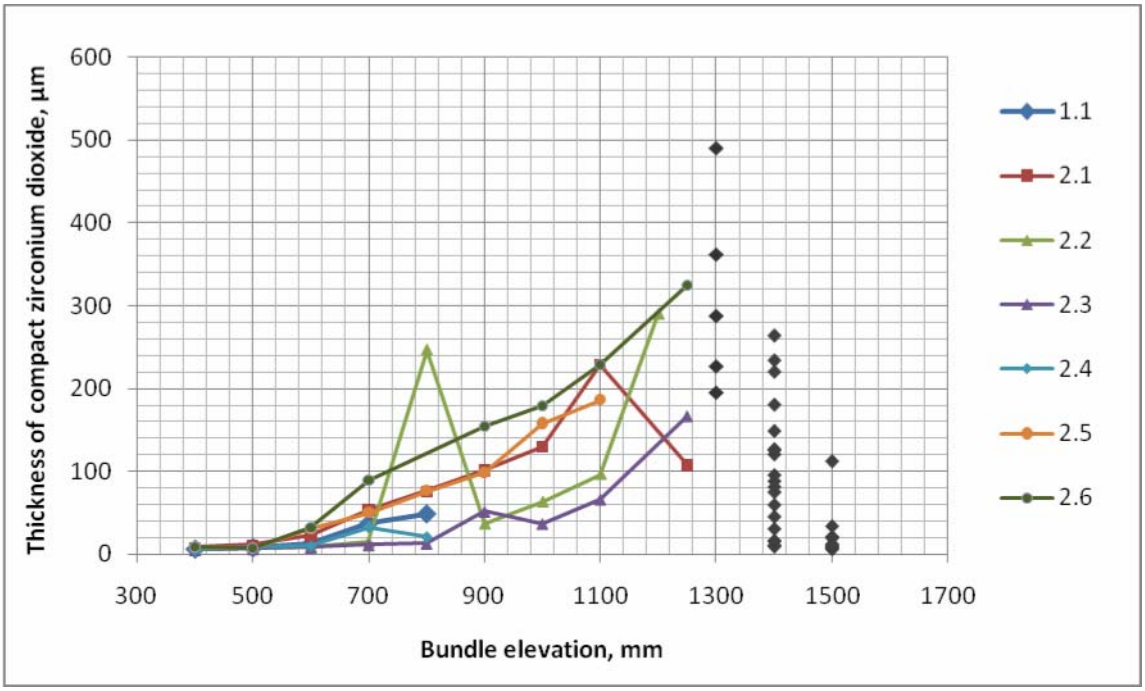

Fig. 35. Distribution of thickness of the compact (measured) ZrO_2 layer on external surface of fuel rods in the second row over the assembly height.

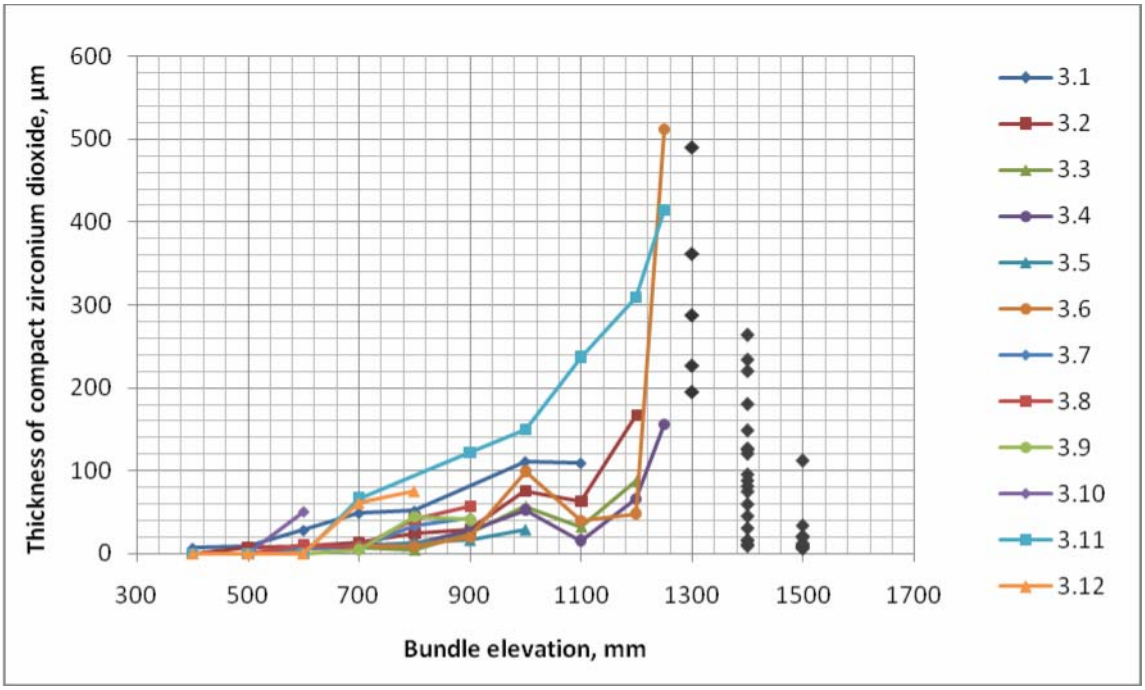

Fig. 36. Distribution of thickness of the compact (measured) ZrO_2 layer on external surface of fuel rods in the third row over the assembly height.

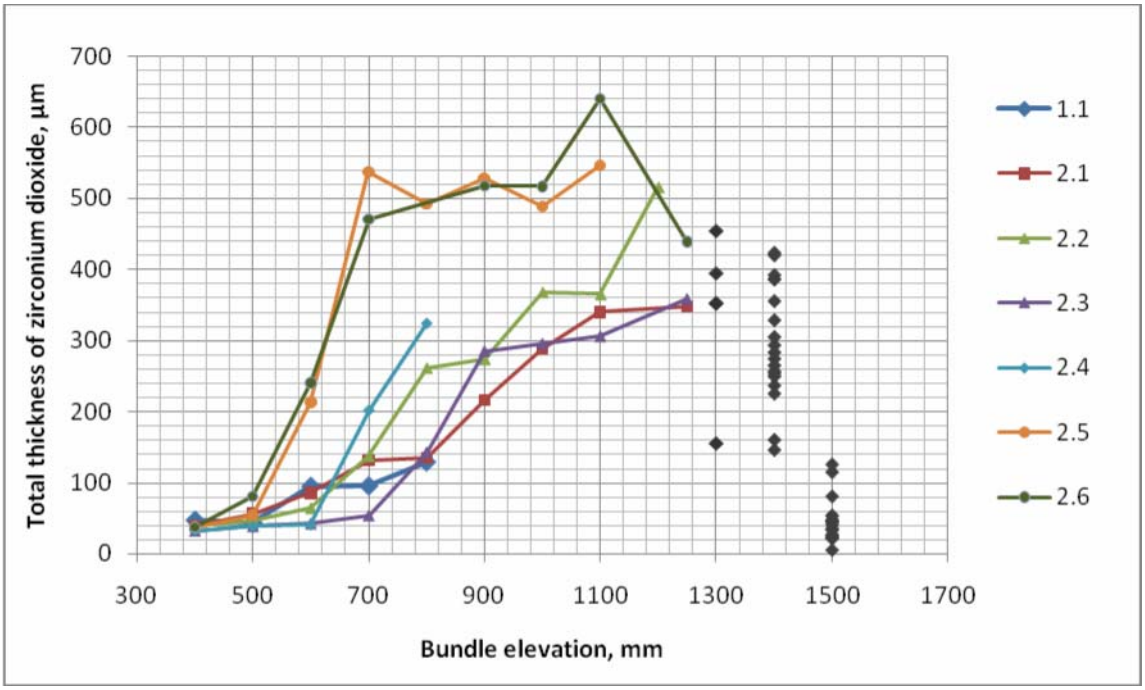

Fig. 37. Distribution of the calculated ZrO_2 thickness on external surfaces of fuel rods in the second row over the assembly height.

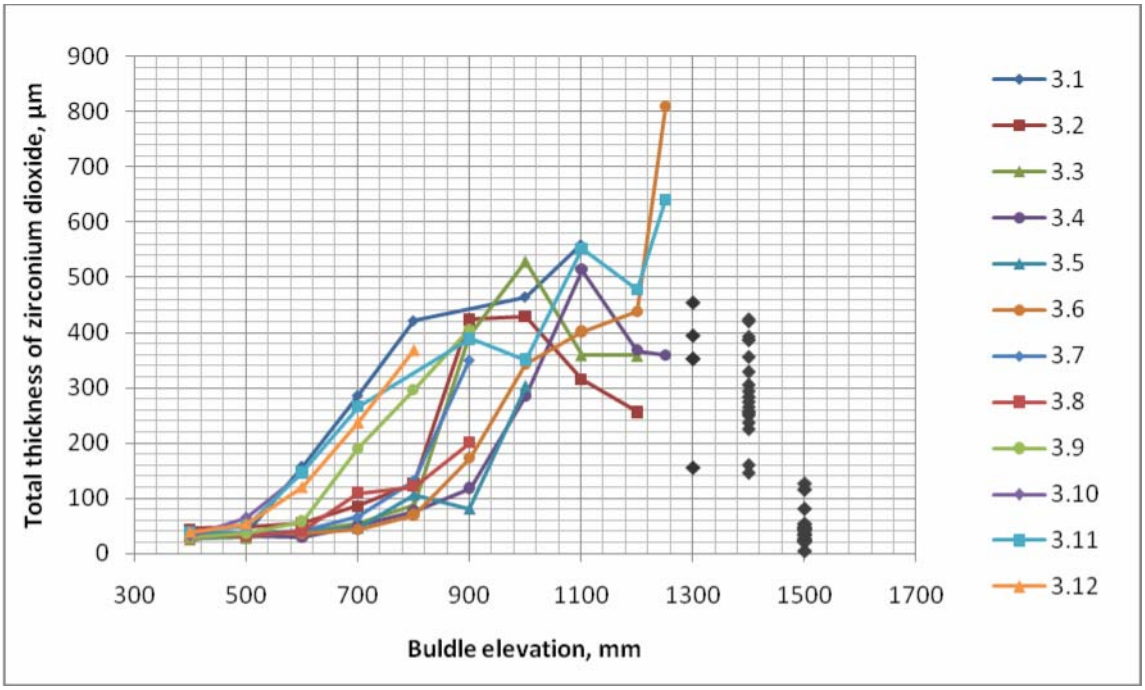

Fig. 38. Distribution of the calculated ZrO_2 thickness on external surfaces of fuel rods in the third row over the assembly height.

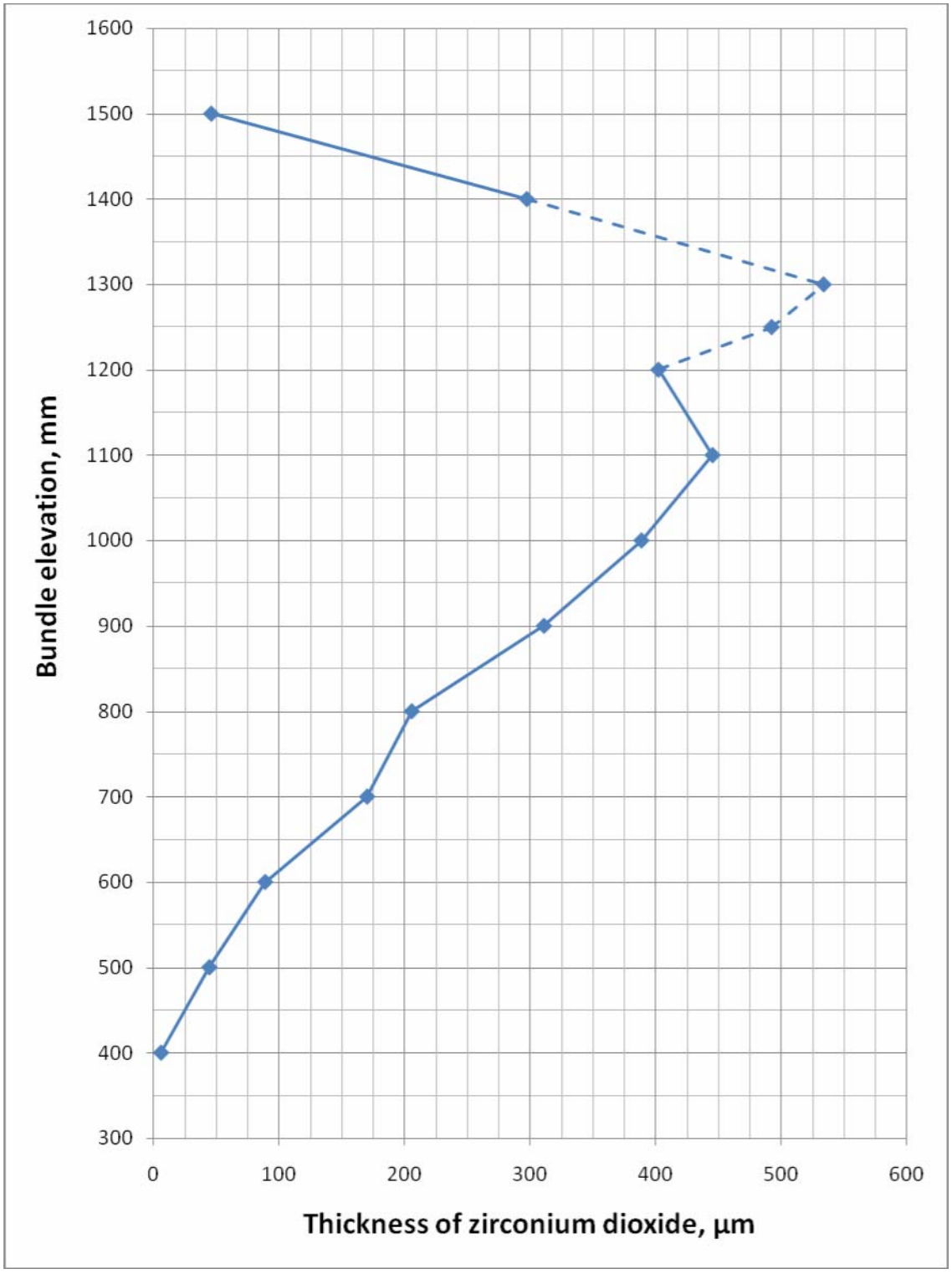

Fig. 39. Distribution of the averaged thickness of calculated oxide scale on cladding surfaces over the assembly height.

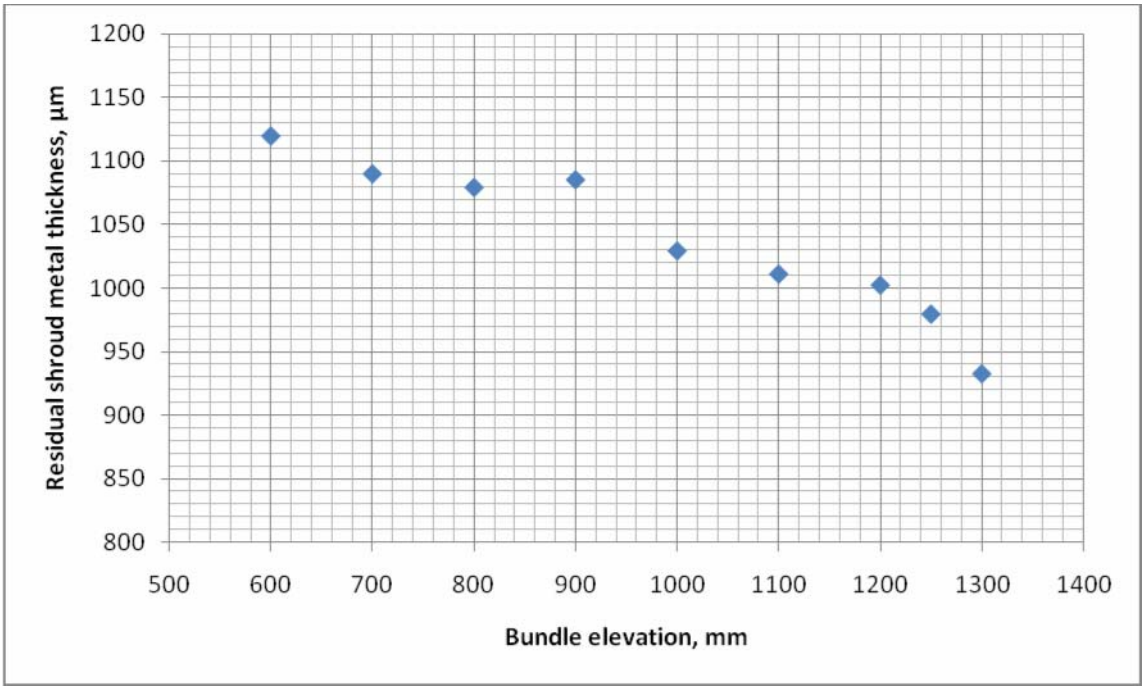

Fig. 40. Distribution of the averaged thickness of the remained metal layer of the shroud over the assembly height.

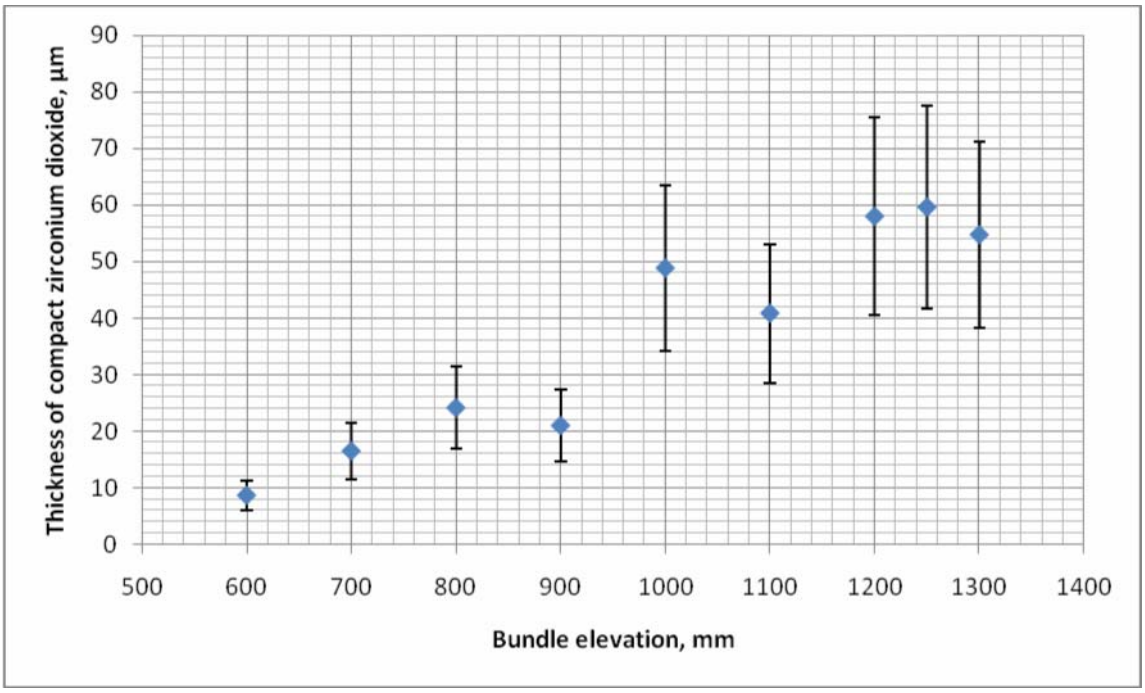

Fig. 41. Distribution of thickness of dense ZrO_2 layer (with indication of minimum and maximum values) on internal surface of the shroud over the assembly height.

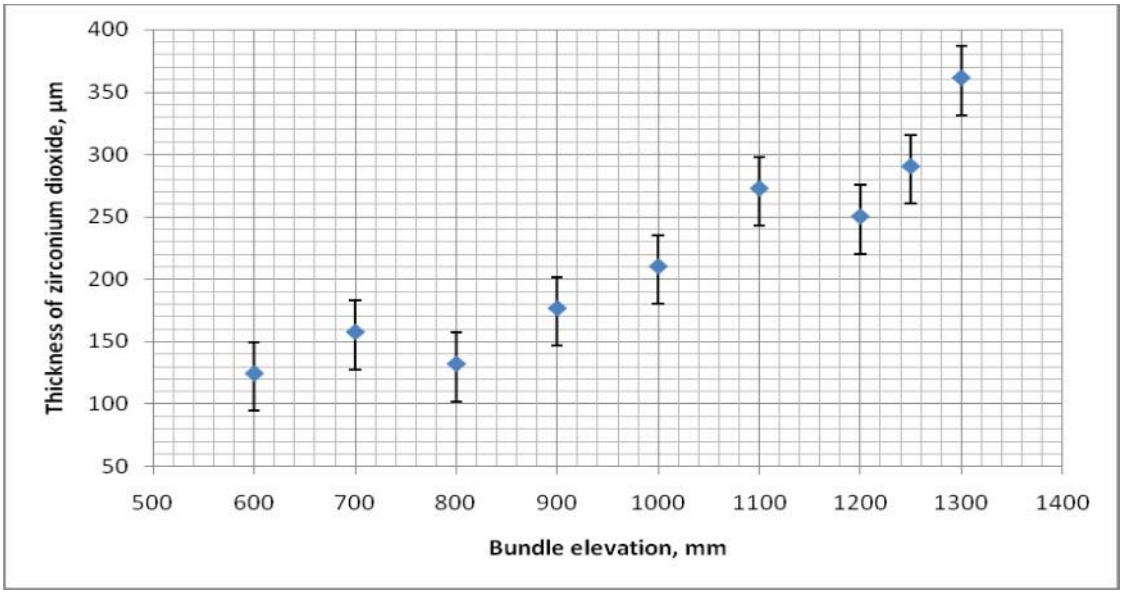

Fig. 42. Distribution of the calculated ZrO_2 thickness on internal surfaces of the shroud (minimum and maximum values corresponds to minimum and maximum shroud wall thickness measured).

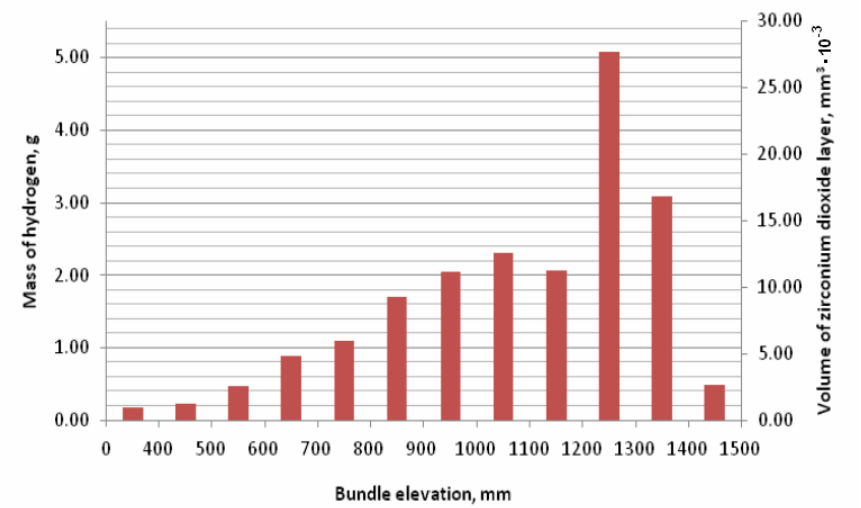

a

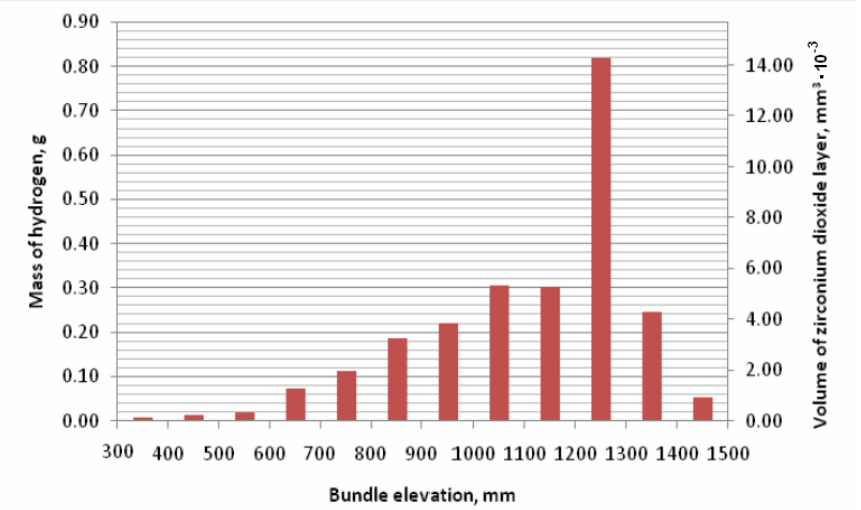

b

Fig. 43. Distribution of specific contributions from cross-sections of model FA into the amount of hydrogen (a – from oxide layers; b – from suboxide layers) generated during oxidation of fuel rods.